DTM-70-5D

Final Report

for

Design and Development of a Prototype Static Cryogenic Heat Transfer System

Contract NAS5-21191

August, 1971

Prepared for

National Aeronautics and Space Administration
Goddard Space Flight Center
Greenbelt, Maryland 20771

dynaTherm CORPORATION
Cockeysville, Maryland 21030

DTM-70-5D

FINAL REPORT

for

DESIGN AND DEVELOPMENT OF A PROTOTYPE STATIC CRYOGENIC HEAT TRANSFER SYSTEM

Contract NAS5-21191

August 1971

Goddard Space Flight Center

Contracting Officer: H. Arista
Technical Monitor : Dr. A. Sherman

Prepared by

Dynatherm Corporation
One Industry Lane
Cockeysville, Maryland

Program Manager: Dr. W. Bienert

for

Goddard Space Flight Center
Greenbelt, Maryland 20771

FOREWORD

This technical report describes the work completed under Contract NAS5-21191, "Design and Development of a Prototype Static Cryogenic Heat Transport System." The program was administered by the Goddard Space Flight Center, Greenbelt, Maryland. Dr. Allan Sherman was the NASA technical officer.

The investigation was conducted by Dynatherm Corporation, Cockeysville, Maryland, under the direction of Dr. W. B. Bienert, Program Manager. Principal investigators were P. J. Brennan and Dr. E. A. Skrabek.

Acknowledgements

The author wishes to express his appreciation to Dr. Sherman for his assistance throughout the program. Special thanks to Dr. William Zisman of Naval Research Laboratory for his time and valuable recommendations regarding contact angle phenomena.

ABSTRACT

This report describes the work completed in the development of a high performance static cryogenic heat transfer system. An analysis was conducted which verified the high performance capability of a "non-wetting cryogenic capillary-pumped-loop." As a result, an investigation was undertaken to determine the feasibility of obtaining a non-wetting cryogenic liquid/solid combination. Results of a literature search indicated that this was feasible for cryogenic liquids provided that low energy solid surfaces are used. Contact angle measurements of liquid nitrogen, oxygen, and Freon 13 on various low energy surfaces were made. The results of these measurements showed that all of the test samples were wet by the different cryogenic liquids; the highest contact angle measured was 30^{o}.

The results of the contact angle measurements did not absolutely rule out the possibility of obtaining a wick structure which is non-wetting with cryogenic liquids. However, in the interest of developing a high-performance static cryogenic heat transfer system within the time limitation of this contract, the development of a heat pipe which utilized a wetting "arterial" wick was pursued. An experimental model whose artery design was optimized to facilitate start-up was fabricated and tested. Nitrogen was used as the working fluid. The experimental model has a heat transport capability greater than 1500 watt-cm which is well in excess of projected requirements for spacecraft applications employing cryogenic heat pipes. Once primed, the heat pipe was relatively insensitive to gravity and was able to support a static elevation head ($q = 0$) of 3.75 cm. Approximately 25 watts of electrical power was transported by the model when oriented in an adverse condition in which the condenser section was 0.25 cm below the evaporator section of the heat pipe. The total temperature drop between the evaporator and the liquid nitrogen bath was $18^{o}C$ for this condition. Repeatable start-up and self-priming was also demonstrated.

TABLE OF CONTENTS

LIST OF ILLUSTRATIONS

LIST OF ILLUSTRATIONS (Continued)

NOMENCLATURE

Symbol	Definition
A	Area normal to the fluid flow
D	Hydraulic diameter
d_a	Artery diameter
g	Gravitational Constant
h	Elevation of evaporator relative to condenser
k	Permeability, Ratio of specific heats
L	Length
L_f	Effective length
$\dot{m}$	Mass flow rate
m	Mass
N	Transport factor
n	+1 if evaporator below condenser -1 if evaporator above condenser
P	Porosity of wick structure
p	Pressure
Q	Volumetric flow rate
q	Heat rate
R	Radius, Gas Constant
R_e	Reynolds Number
r	Average pore radius of wick structure
r_p	Effective pumping radius
T	Temperature
W_A	Work of adhesion
t	Thickness of wick structure
θ	Contact angle
λ	Heat of vaporization
μ	Viscosity
ν	Kinematic viscosity
ρ	Density

Symbol	Definition
C	Tortuosity factor
β	Defined by Eq. (2-19)
ϵ	Defined by Eq. (2-12)
σ	Surface tension
φ	Defined by Eq. (2-6)
Ψ	Defined by Eq. (2-20)

Subscripts

C	Condenser, Critical
CH	Gas dynamic choking
E	Elevation
e	Evaporator
g	Gas
i	Inner
L	Liquid
LV	Liquid in equilibrium with its vapor
max	Maximum
OP	Open artery
p	Capillary pumping
st	Storage volume
T	Transport section
V	Vapor
W	Wick structure

Section 1

INTRODUCTION

Cryogenic heat pipes, as yet, have not been reduced to practice. The purpose of this research program was to determine the feasibility of a static cryogenic heat transfer system which is relatively insensitive to gravity and has a high heat transport capability. These requirements lead to a heat pipe which employs a composite wick structure. This type of wick is characterized by having high capillary pumping and low viscous losses for the liquid flow. A particularly attractive configuration for cryogenic application consists of a capillary-pumped loop with a non-wetting pumping surface at its condenser section. In addition to possessing the features of a composite wick, a design of this type has the potential advantage of simplifying start-up in a cryogenic heat pipe.

An analytic investigation was performed to determine the feasibility of a non-wetting capillary pumped loop. The maximum heat transport capability ($q L_f$) was determined taking into account the sonic vapor limitation as well as the more common capillary pumping limit. Results of the analysis indicate that a non-wetting cryogenic capillary-pumped loop is feasible and has a maximum heat transport capability in excess of 5000 watt-cm in the horizontal position. The static wicking height would be 100 cm or greater with this system even for very shallow non-wetting contact angles.

The use of a non-wetting pumping surface requires that the contact angle between the working liquid and the capillary structure be greater than ninety degrees. Practically all previous contact angle measurements had been performed at room temperature; there is essentially no mention of cryogenic contact angle data in the literature. As a result, in order to evaluate the feasibility of a non-wetting system it was necessary to perform

cryogenic contact angle measurements. To this end, an extensive literature survey was conducted to establish what solid-cryogenic liquid combinations have the greatest potential for non-wetting. Results of the survey indicated that non-wetting by cryogenic liquids should be feasible and that the most promising solid surfaces are those which have a very low surface energy or critical surface tension. The lowest surface energies are obtained for perfluoroacid monolayers deposited on a metallic substrate. Teflon and polyethylene as well as several low energy coatings also qualify. Clean metallic surfaces have very high surface energies and are wetted by most liquids.

Contact angle measurements of liquid nitrogen, oxygen, and Freon 13 on the various low energy surfaces and on reference high energy surfaces were performed. The "tilting plate" method was used to establish the contact angle. The experimental results showed that all of the test samples were wet by the different cryogenic liquids; the highest contact angle measured was 30^{o}. This was obtained for liquid nitrogen on a monolayer of perfluorodecanoic acid. Most of the surfaces tested exhibited contact angles which were less than 15^{o}. It is possible that the room temperature results and related theory are not applicable at cryogenic temperatures. The very low contact angles could also be explained by the existing theory if the critical surface tension of the solid had increased in the cryogenic temperature regime. Another possibility suggested by Zisman* is that there are impurities such as neon, argon, etc., in the cryogenic test liquids which could have reduced their surface tensions considerably and therein the potential for non-wetting.

The cryogenic contact angle measurements do not absolutely rule out the feasibility of obtaining non-wetting cryogenic liquid/solid combinations. However, in the

*Dr. Zisman is an administrator of the Naval Research Laboratory's Chemical Division and is a leader in the field of Surface Chemistry.

interest of developing a high-performance static cryogenic heat transfer system within the time limitation of this contract further contact angle measurements were not made, and the development of a heat pipe which utilized a wetting "arterial" wick structure was pursued. The arterial design was chosen because its ability to operate as a composite wick had been demonstrated with conventional heat pipe fluids.[1] An experimental model containing an artery which was optimized to facilitate start-up with liquid nitrogen was fabricated and tested. The artery has a 1.6 mm diameter and was formed from 200 mesh stainless steel screen. It is contained in an aluminum tube (1.27 cm O.D. x 91 cm long) which was threaded internally over its length to provide circumferential distribution of the working liquid. The heat pipe was wrapped with super-insulation and tested in a thermal vacuum chamber whose walls were at room temperature. Heat was dissipated at the condenser section to a liquid nitrogen bath at atmospheric pressure. Liquid nitrogen was also used as the heat pipe working fluid.

Results of the tests demonstrate that a cryogenic wetting arterial heat pipe is feasible as well as practical. Performance data indicate that the maximum transport capability of this particular design is greater than 1500 watt-cm in a "1g" environment. The data also shows that the system can support a 3.5 cm static elevation head of liquid nitrogen. Approximately 25 watts of electrical power was transported by the model when oriented in an adverse condition in which the condenser section was 0.25 cm below the evaporator section of the heat pipe. The total temperature drop between the evaporator and the liquid nitrogen bath was 18^{o}C for this condition. Repeatable start-up and self-priming was also demonstrated.

It is recommended that further tests be conducted with the existing heat pipe to establish the self-starting reliability and to obtain basic information related to its

heat transport capability. In addition, the present design could be modified to improve its overall performance.

Section 2

ANALYTIC INVESTIGATION OF A NON-WETTING HEAT PIPE SYSTEM

The projected maximum transport requirement ($q \cdot L_f$) for cryogenic heat pipe applications is on the order of 1000 W-cm. It would seem that this requirement would be easy to achieve, particularly when ambient heat pipes have been tested to approximately 10^5 W-cm.[1] However, for cryogens, the liquid transport factor (N_L), which is a measure of heat transport capability, is more than an order of magnitude lower than for common ambient temperature fluids. In addition, cryogenic liquids have relatively low surface tensions and slight misorientations in a gravity field can seriously detract from the performance of cryogenic heat pipes. The requirements for a high-performance static cryogenic heat transfer system which is relatively insensitive to gravity fields has directed the investigation to a heat pipe which employs a "composite wick structure."* Although a composite wick can provide high heat transport capability, it does have potential start-up problems. To facilitate start-up of a cryogenic heat pipe a non-wetting wick structure was selected. A non-wetting wick structure permits full capillary pumping to be established in the condenser section.

This section presents a qualitative evaluation of a non-wetting heat pipe which employs a composite wick and a parametric analysis for predicting the maximum transport capability of such a system.

A. Qualitative Evaluation

The high heat transport capability of a composite wick is realized because the

---

*The generic term "composite" is used to define a wick structure for which the capillary pumping is independent of the bulk liquid flow between the evaporator and the condenser.

capillary pumping and the bulk liquid flow are independent of each other. Consequently, a large pumping pressure can be obtained without incurring excessive viscous flow losses. Minimizing the viscous flow losses without sacrificing high capillary pumping pressure results in a heat pipe which has high heat transport capability and is relatively insensitive to gravity.

In order to approach the performance capability of a composite wick heat pipe, the liquid flow area of a homogeneous wick must be significantly larger. As a result, a homogeneous wick heat pipe of comparable performance will have a larger liquid inventory than that required for a composite wick heat pipe. In addition to increased weight associated with the additional fluid inventory, the homogeneous wick heat pipe tube or pressure vessel will be heavier. The heavier wall is required in order to contain the higher pressures at super critical temperatures associated with the extra fluid.

While a composite wick offers maximum performance and minimum weight, it does have potential start-up problems. Prior to start-up of a cryogenic heat pipe, the working fluid will be gaseous. Start-up is initiated by removing heat from the condenser section. After the onset of condensation of the working fluid in the condenser section the liquid begins to fill the wick and gradually advances toward the evaporator section. As the liquid advances, it evaporates and thereby cools the downstream portion of the heat pipe and compensates for parasitic heat leaks. The rate at which the liquid advances at any instant is determined by the same pressure balance that establishes the steady-state heat transport capability of a heat pipe,[2]

$$\Delta p_p = \Delta p_V + \Delta p_L + \Delta p_E \qquad (2\text{-}1)$$

That is, the rate at which heat can be transported is determined by a balance between the capillary pumping pressure and the liquid and vapor viscous pressure drops and any

elevation head that exists. Maximum capillary pumping is not available in a wetting composite wick until the liquid channels have been completely filled.[1] The capillary pumping of a partially filled composite wick is determined by the relatively large diameter of the liquid channels and is generally more than an order of magnitude less than the pumping available when the wick is filled. Consequently, priming of a composite wick can be difficult if the heat leaks are excessive and/or if an adverse elevation (condenser below the evaporator) exists.

The use of a non-wetting wick structure in the condenser section will permit full pumping upon the onset of condensation of the working fluid. The principle of operation of a non-wetting heat pipe is basically the same as for a conventional heat pipe and can be best explained by referring to the basic mechanism of capillary pumping. A wetting liquid will tend to fill the pores of a wick structure or a capillary tube and form a meniscus which is convex toward the liquid as shown in Figure 2-1a. A non-wetting liquid, on the other hand, will tend to be repelled by the solid structure and the meniscus will appear as shown in Figure 2-1b.

In both cases, the curvature of the liquid-vapor interface results in a pressure difference between liquid and vapor, given by

$$p_V - p_L = \frac{2\sigma \cos\theta}{r_p} \qquad (2\text{-}2)$$

For a non-wetting liquid the contact angle (θ) is greater than 90^o and the pressure in the vapor is less than that of the liquid by an amount given by the above equation. The utilization of this pressure difference for circulating the working fluid in a heat pipe is well established. As indicated in Figure 2-1b, pumping with a non-wetting fluid occurs at the condenser as the liquid is repelled from the wick structure. Thus, in a cryogenic

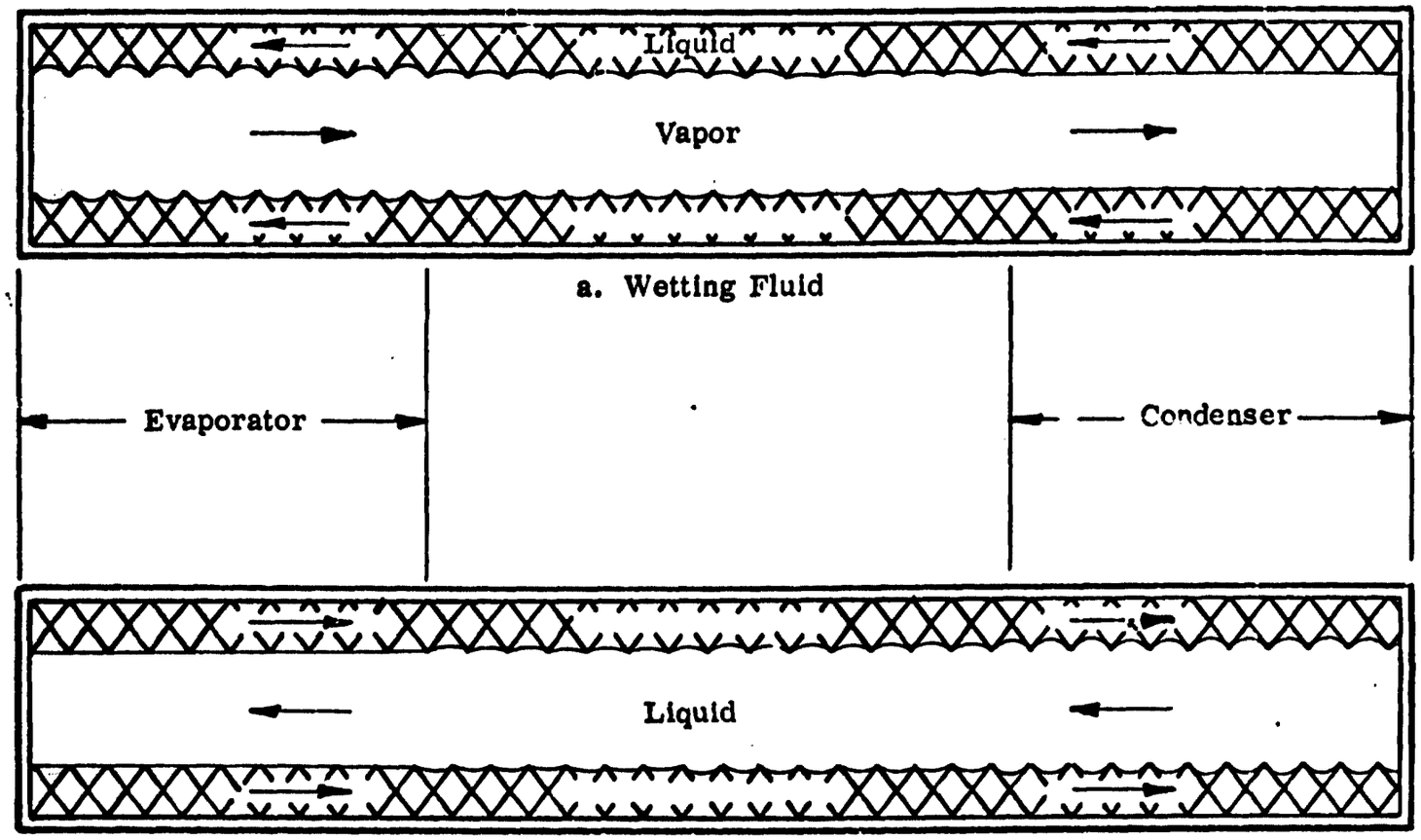

FIGURE 2-1

HEAT PIPE PRINCIPLE

heat pipe, maximum capillary pumping can be established as soon as the condensing liquid begins to saturate the wick.

B. Analysis

A schematic of the potential non-wetting heat pipe system which was selected for analysis is shown in Figure 2-2. The system is generally referred to as a "capillary pumped loop", and its operation is derived from the composite wick principle. A non-wetting porous wick structure is located within the condenser section and provides the main capillary pumping. A wetting wick structure is located in the evaporator section and its purpose is primarily to provide circumferential distribution of the liquid. The transport of liquid and vapor between the evaporator and condenser sections takes place through low-pressure-drop capillary tubes.

The analysis of a cryogenic non-wetting capillary pumped loop is essentially the same as for conventional heat pipes. The maximum heat transport capability is determined by establishing which of the following mechanisms result in a burn-out of the heat pipe.

(1) Heat Flux Limitation (Superheating)

At the superheating limit, hot spots form in the evaporator as a direct consequence of exclusion of liquid due to boiling in the capillary structure.

(2) Transport Limitations

In these limits, various failure mechanisms result in insufficient return of condensate liquid to the evaporator. Generally this will result from

(a) limited capillary pumping (i.e., excessive viscous flow losses),

(b) sonic vapor velocities,

(c) excessive interfacial shear between liquid and vapor, and

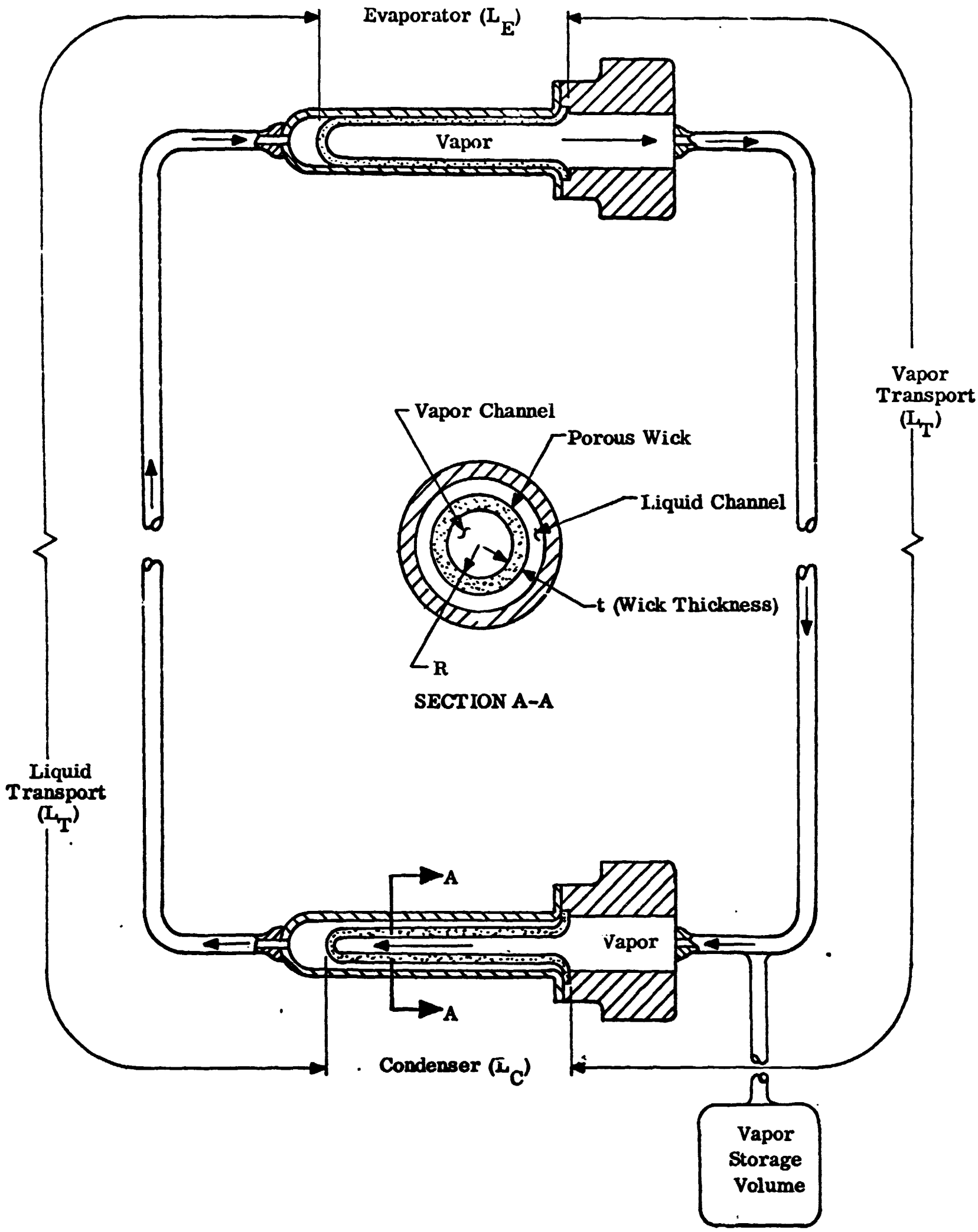

FIGURE 2-2. NON-WETTING CAPILLARY PUMPED LOOP

(d) entrainment of liquid droplets in the vapor flow.

Proper design of the evaporator wick will prevent nucleate boiling at the heat fluxes associated with cryogenic applications, and therefore the superheating mechanism should not dominate. In addition, because of the basic geometry of a capillary pumped loop, failure due to transport limits resulting from (c) and (d) will not occur. Thus the maximum heat transport capability for this system will be determined by either the well-known capillary pumping limit or the sonic vapor flow limitation.

1. Capillary Pumping Limitation

As in the case of conventional heat pipes, the q_{max} associated with the capillary pumping limit is determined by equating the maximum capillary pressure to the sum of the viscous pressure drops (both in liquid and vapor) and the elevation head when in a gravity field,

$$\Delta p_{p_{max}} = (\Delta p_V + \Delta p_L)_W + (\Delta p_V + \Delta p_L)_T + \Delta p_E \qquad (2\text{-}3)$$

The quantity Δp_E is the pressure drop due to the elevation of the evaporator relative to the condenser in a gravity environment. For a capillary pumped loop, the static pumping head that can be established by the fine porous wick structure is quite large (~100 cm), and the elevation term can be neglected. The capillary pumping in the evaporator section is used only to provide circumferential distribution of the liquid there and is negligible compared to that established in the condenser wick. Thus the maximum capillary pressure in a non-wetting system is given by

$$\Delta p_{p_{max}} = (p_L - p_V)_C = \frac{-2\sigma \cos\theta}{r_{p_{min}}} \qquad (2\text{-}4)$$

The viscous losses in the transport section are the same as for conventional heat pipes and are given by[2]

$$\Delta p_{L_T} = \left(\frac{32 \mu L_T q}{\rho \lambda D^2 A} \right)_L$$

$$\Delta p_{V_T} = \varphi \left(\frac{32 \mu L_T q}{\rho \lambda D^2 A} \right)_V \qquad (2\text{-}5)$$

where the factor φ depends on whether the vapor flow is laminar or turbulent:

$$\varphi = \begin{cases} 1 \text{ when } Re_V \leq 2200 & (2\text{-}6a) \\ 5.9 \times 10^{-3} \left(\frac{q}{D \mu \lambda} \right)_V^{3/4} \text{ when } Re_V > 2200 & (2\text{-}6b) \end{cases}$$

Because of the relatively small diameters of a capillary pumped loop the vapor flow in the transport section will generally be turbulent and Eq. (2-6b) is applicable.

The fluid flow through the porous wick structures in the evaporator and condenser sections represents flow through porous media and is described by Darcy's Law. In order to simplify the analysis it is assumed that the fluid flows only in the radial direction through the wick, and also that the heat is added/removed uniformly at these sections. These assumptions result in a radial mass flow through the wick structure which is uniform along the length of the evaporator and the condenser.

Darcy's Law for a radial fluid flow which is uniform over the cross-sectional area of the porous media normal to the flow is stated as[3]

$$Q = \frac{-kA_W}{\mu} \frac{dp}{dR} \tag{2-7}$$

where $A_W = 2\pi R L_W$ (2-8)

and $Q = \frac{\dot{m}}{\rho} = \frac{q}{\lambda \rho}$ (2-9)

As a first approach, it is assumed that the porous media is represented by a bundle of capillaries in which case the permeability is given by

$$k = C P r_p^2 \tag{2-10}$$

where P = Porosity of the wick

and C = Non-dimensional constant which is related to the tortuosity of the capillaries as well as the type of capillaric model which is chosen.

Subject to the above assumptions, the radial pressure drop through a porous wick is given by

$$\Delta p_W = \frac{q}{\varepsilon r_p^2 L_W} \left(\frac{\nu}{\lambda}\right) \ln\left(1 + \frac{t}{R_i}\right) \tag{2-11}$$

where $\varepsilon \equiv C\pi P$ (2-12)

In the temperature regime of interest ($T \sim 77^{\circ}K$), the kinematic viscosity of the vapor (ν_v) is an order of magnitude or greater than that of the liquid for the fluids being considered. This coupled with the relatively large pore size, which would be adequate to provide circumferential distribution of the liquid in the evaporator, results in a negligible liquid pressure drop through the

evaporator wick. Finally, in applications where a capillary pumped loop is employed the length of the transport sections will be substantially larger than either the evaporator or condenser lengths. Consequently, the major viscous losses in a capillary pumped loop will be associated with the fluid flow in the transport sections, and the vapor flow through the fine pore wick structure in the condenser. Thus for a non-wetting capillary pumped loop, the maximum heat transport associated with the pumping limit is determined from

$$q_{max} = \frac{\cos\theta}{16\, r_p}\, N_V\, \frac{(D_V^2\, A_V)_p}{\nu_T}\, F \qquad (2\text{-}13)$$

where N_V is the vapor transport factor

$$N_V \equiv \frac{\sigma\lambda}{\nu_V} \qquad (2\text{-}14)$$

and

$$F = \left\{ \frac{\nu_L}{\nu_V} \left(\frac{D_V^2\, A_V}{D_L^2\, A_L} \right) + 2 + \frac{(D_V^2\, A_V)_T \ln\left(1 + \frac{t}{R_i}\right)}{\varepsilon\, r_p^2\, L_T\, L_W} \right\}^{-1} \qquad (2\text{-}15)$$

In order to reduce heat leaks as well as the system's weight it is desirable to minimize the diameter of the transport sections. Ideally the parameter $\frac{t}{R_i}$ should be made as small as practical in order to obtain good heat transfer at the condenser as well as minimizing the viscous losses through the porous wick. Also, for a specified liquid/surface combination and operating temperature, the properties associated with the wick (ε, θ) as well as the physical properties of the fluid will be fixed. In addition, the lengths of the transport and condenser sections will be specified for a particular application. As a result, an evaluation of Eqs. (2-13) and (2-15) indicates that for a given application and choice of working

fluid and wick material the required pumping radius (pore size) is determined from

$$r_p = r_p\,(D_V,\ D_L) \tag{2-16}$$

Equations (2-13) and (2-15) were combined to solve for D_V, and D_V was differentiated with respect to r_p in order to minimize the vapor diameter. It was assumed in performing the minimization that the liquid loss in the transport section is negligible and thus the pumping radius is a function only of the vapor transport channel. This assumption is valid provided that the diameters of both the liquid and vapor transport sections are approximately equal. The following relationships for r_p and D_V were derived from this minimization.

$$(r_p \cos\theta)_{min} = \frac{q_{max}}{N_V}\left(\frac{1}{2\,L_W\beta}\right) \tag{2-17}$$

and

$$D_{V_{min_p}} = 0.553\left\{\left(\frac{q_{max}}{\mu\lambda}\right)_V^{3/4}\left(\frac{L_T}{L_W}\right)\left(\frac{q_{max}}{N_V}\right)^2\psi\right\}^{4/19} \tag{2-18}$$

with

$$\beta = \frac{\varepsilon}{\ln\,(1 + t/R_i)} \tag{2-19}$$

$$\psi = \frac{\beta}{\cos^2\theta} \tag{2-20}$$

The above equations correspond to having the viscous pressure drop of the vapor in the condenser wick equal to the loss through the vapor transport section, i.e.,

$$\Delta p_p = \Delta p_{V_W} + \Delta p_{V_T} = 2\Delta p_{V_W} \tag{2-21}$$

Results using Table 2-1 properties, are given in Figures 2-3 through 2-8 for

TABLE 2-1

PHYSICAL PROPERTIES OF SELECTED CRYOGENIC FLUIDS

Property	Fluorine T (°K)				Nitrogen T (°K)				Oxygen T (°K)			
	65	70	75	80	65	70	75	77.3	65	70	75	80
σ (dynes/cm)	19.2	17.8	16.3	14.9	11.7	10.5	9.39	8.85	19.6	18.3	17.0	15.7
λ (w-sec/gm)	189	183	177	171	214	208	202	198	234	230	227	223
ρ_L (g/cc)	1.64	1.60	1.58	1.54	.861	.840	.818	.808	1.26	1.24	1.22	1.19
$\rho_V (10^{-4}$ g/cc)	1.18	7.7	17.4	33.0	10.0	18.6	34.0	43.0	.31	1.1	3.8	10.0
$\nu_L (10^{-3}$ cm^2/sec)	2.87	2.45	2.10	1.83	3.25	2.62	2.13	1.96	3.56	2.91	2.39	2.10
$\nu_V (10^{-2}$ cm^2/sec)	17.1	7.0	3.23	1.88	4.4	2.64	1.57	1.28	525	50	15.2	6.1
$N_L (10^6$ w/cm^2)	1.26	1.33	1.37	1.39	.767	.836	.89	.897	1.29	1.45	1.61	1.67
$\nu_L/\nu_V (10^{-2})$	1.69	3.5	6.57	9.75	7.4	9.9	13.7	15.3	0.068	0.38	1.57	3.44
$N_V (10^4$ w/cm^2)	2.12	4.65	9.0	13.5	5.67	8.29	12.2	13.7	0.088	0.84	2.52	5.75

FIGURE 2-3

MAXIMUM HEAT TRANSPORT ASSOCIATED WITH CAPILLARY PUMPING LIMIT

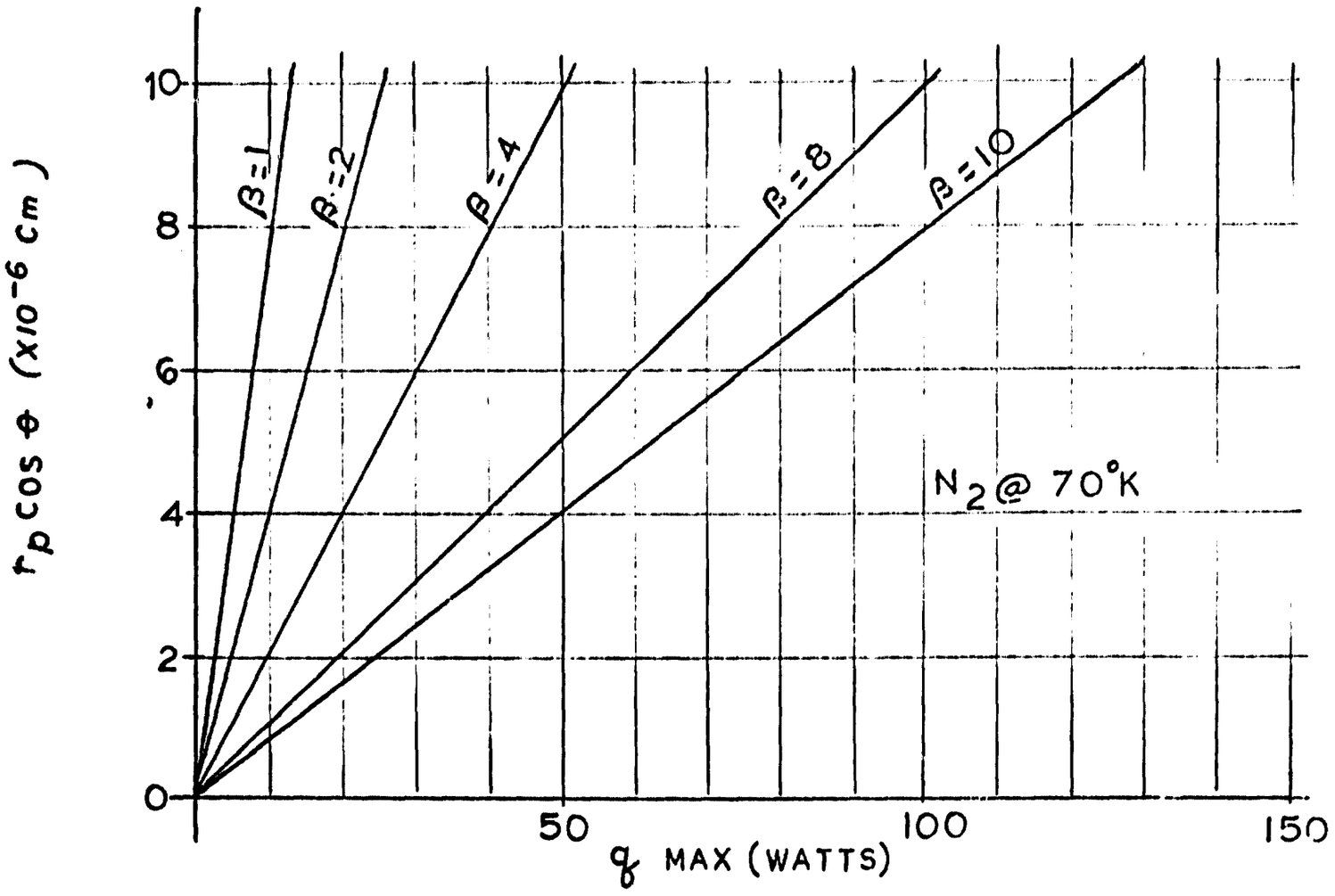

FIGURE 2-4

MINIMUM DIAMETER OF VAPOR TRANSPORT SECTION
ASSOCIATED WITH CAPILLARY PUMPING LIMIT

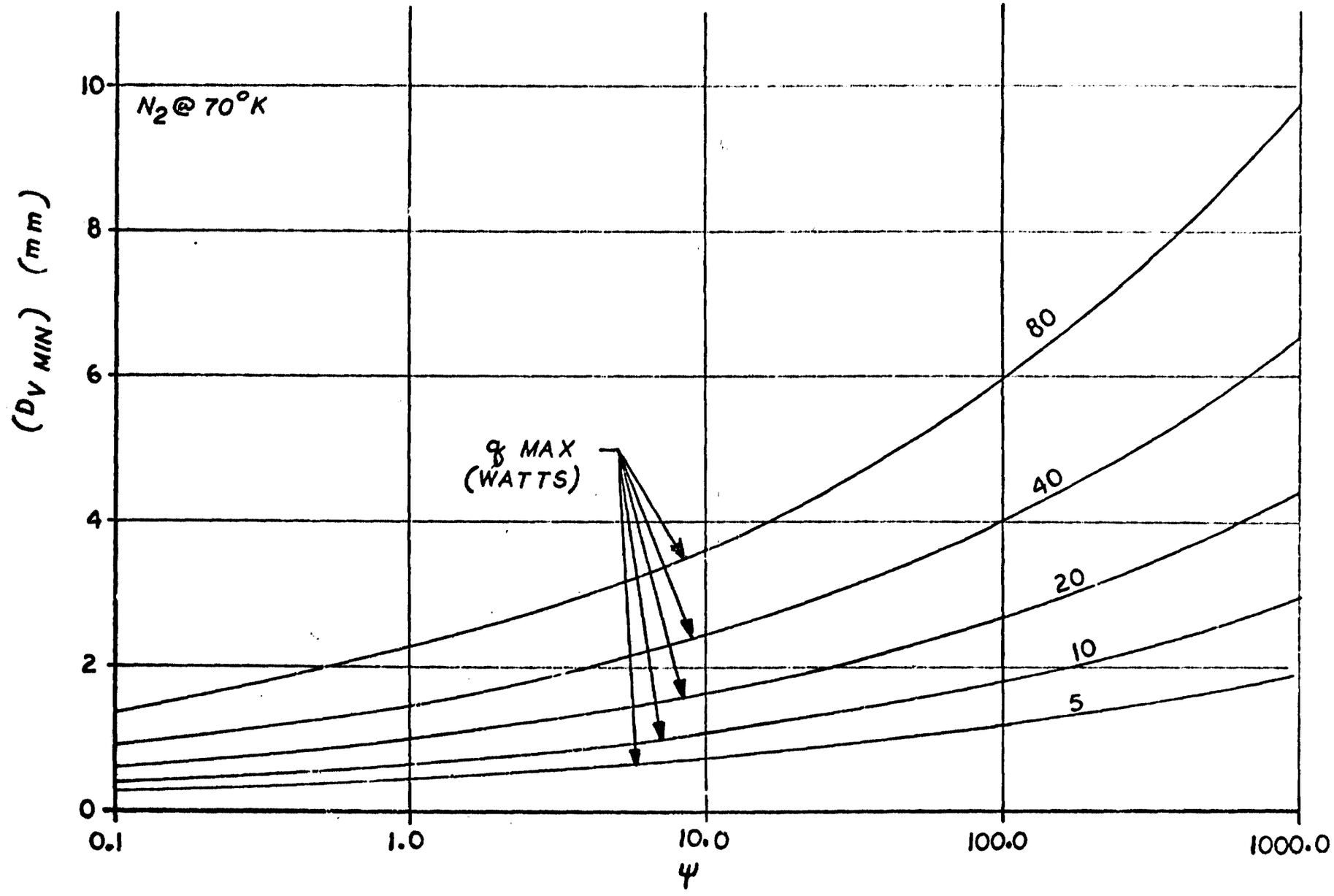

FIGURE 2-5

MAXIMUM HEAT TRANSPORT ASSOCIATED WITH CAPPILLARY PUMPING LIMIT

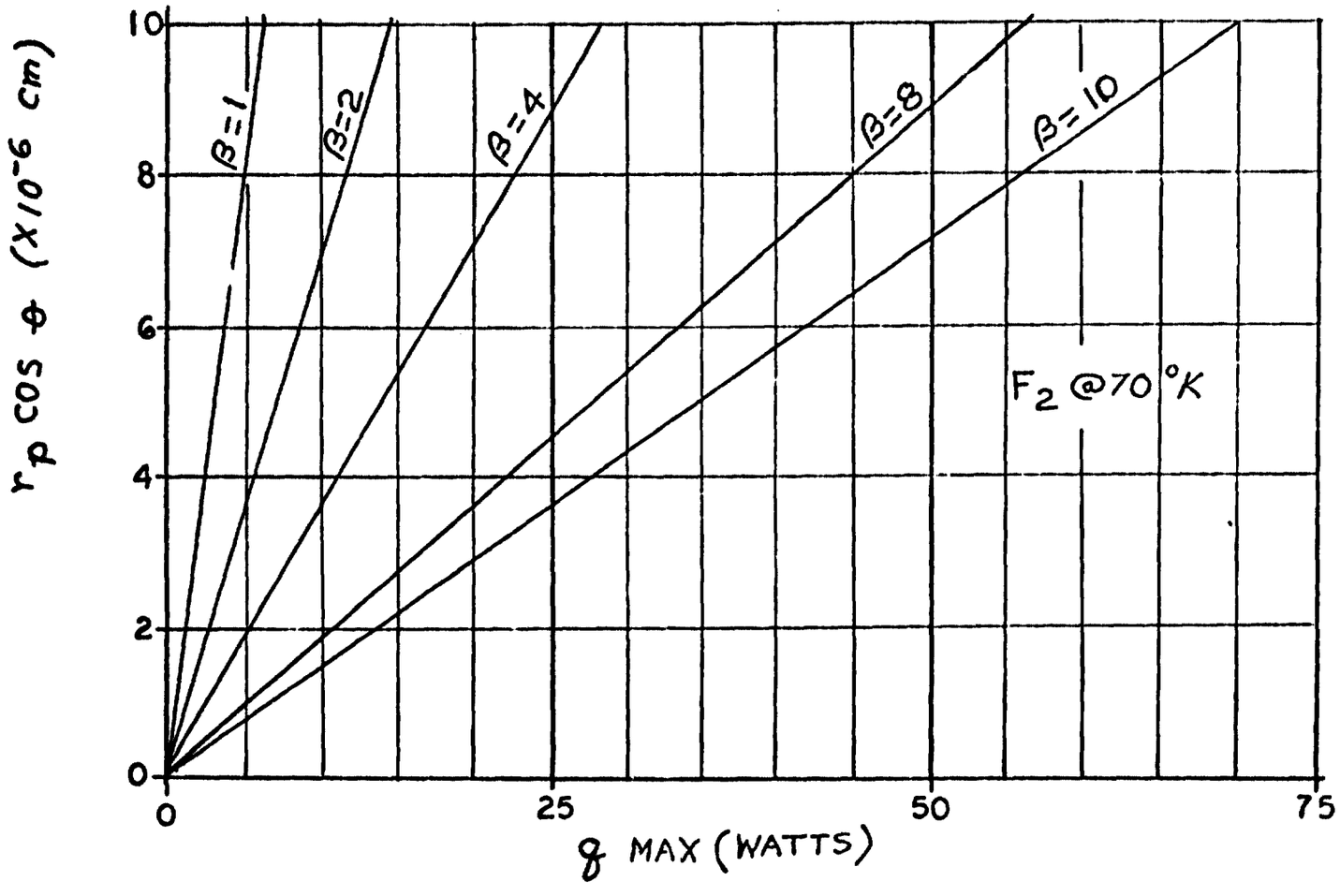

FIGURE 2-6

MINIMUM DIAMETER OF VAPOR TRANSPORT SECTION ASSOCIATED WITH CAPILLARY PUMPING LIMIT

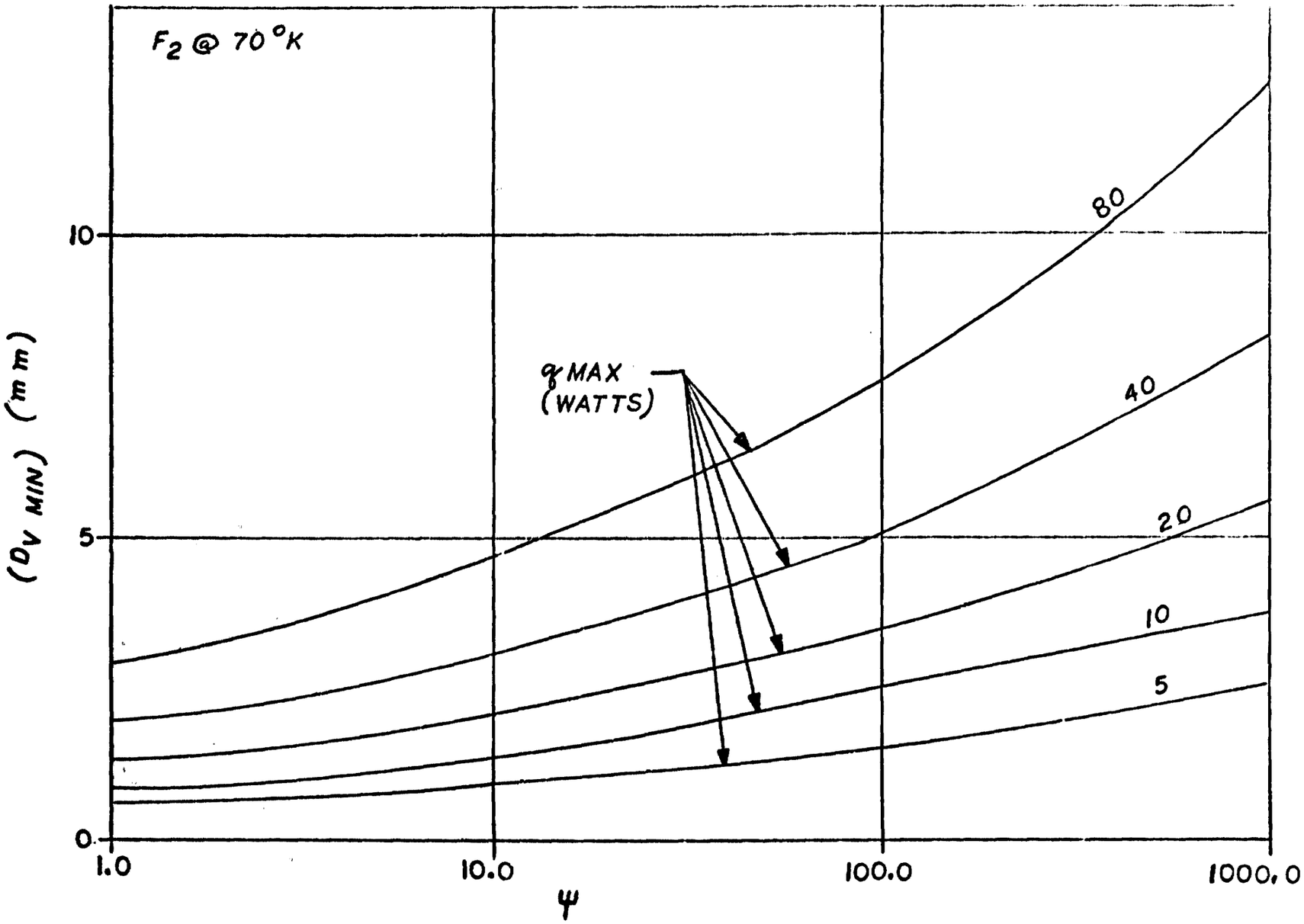

FIGURE 2 - 7

MAXIMUM HEAT TRANSPORT ASSOCIATED WITH CAPPILLARY PUMPING LIMIT

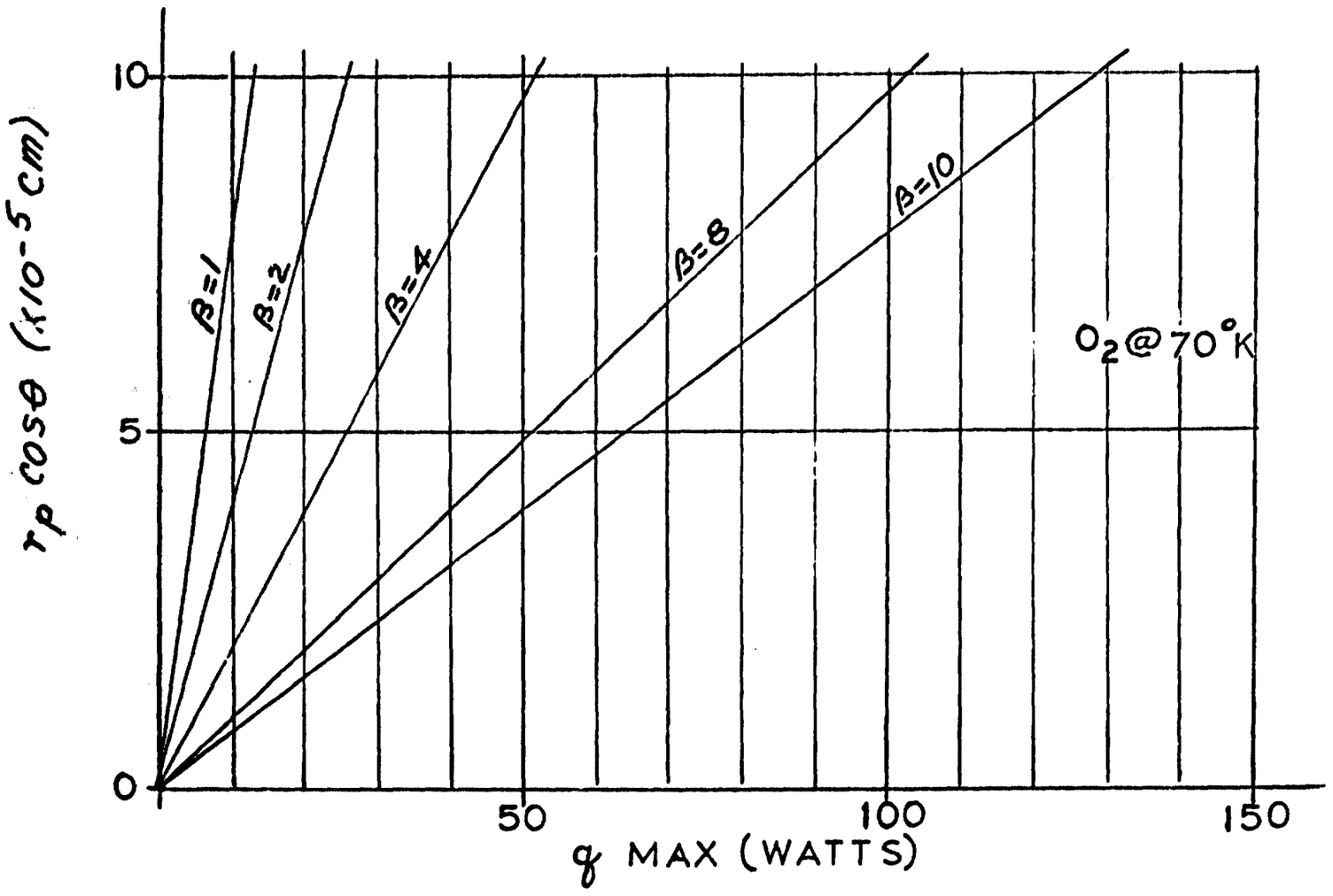

FIGURE 2-8

MINIMUM DIAMETER OF VAPOR TRANSPORT SECTION ASSOCIATED WITH CAPILLARY PUMPING LIMIT

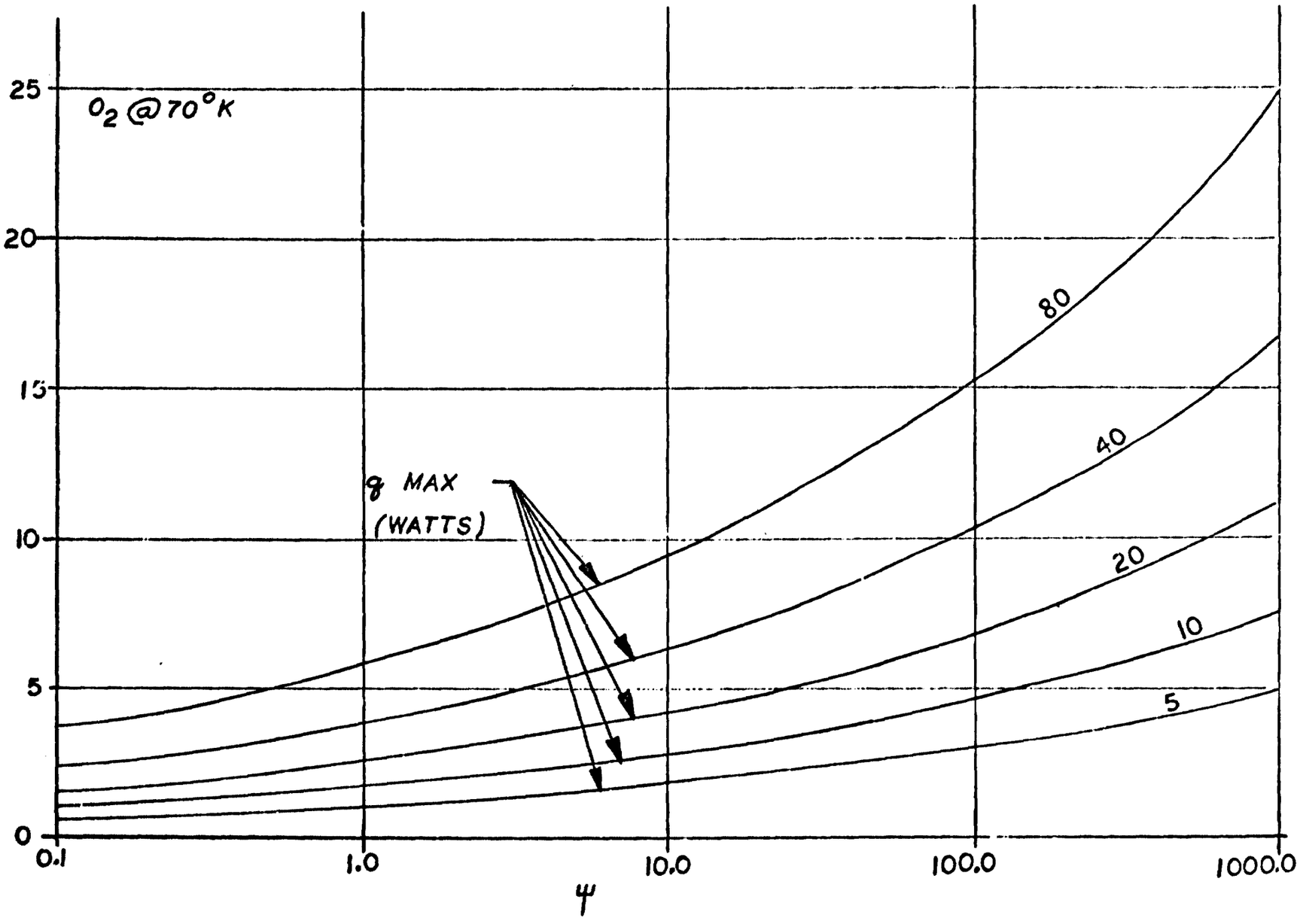

a bulk fluid temperature of 70°K. These results were obtained using a transport length (L_T) and a condenser length (L_W) which are applicable to the ICICLE[4] system

$$L_T = 152 \text{ cm (60 in)}$$

$$L_W = 7.62 \text{ cm (3 in)}$$

For a specified q_{max} and wick geometry the required magnitude of $(r_p \cos \theta)_{min}$ is largest for oxygen and smallest for nitrogen. This is due to the fact that this parameter varies inversely as the vapor transport factor N_V. Consequently, for a given pore size the required degree of non-wetting is lowest for nitrogen and greatest for oxygen. Or correspondingly, because of the higher vapor transport factor of nitrogen the pumping requirement is lowest for a given application and wick structure using this fluid. Similarly, provided that approximately the same contact angle is obtained for each of the three fluids with a given material, the results indicate that the minimum diameter of the vapor section is substantially smaller for nitrogen than for either fluorine or oxygen. Again this is due to the higher value of the vapor transport factor associated with nitrogen. More specifically, the higher value of N_V for nitrogen is due to the fact that the kinematic viscosity of its vapor is lower than for the other fluids. This in turn results in lower viscous losses and correspondingly smaller pumping requirements for a given geometry and application.

The effect of temperature on the required pore size is readily obtained as

$$\frac{r_p \cos \theta}{(r_p \cos \theta)_{70}} = \frac{N_{V_{70}}}{N_V} \qquad (2\text{-}22)$$

where $(\,)_{70}$ implies conditions at $70^{\circ}K$.

Similarly, the effect of temperature on the minimum diameter of the vapor transport section is determined from Eq. (2-18) to be

$$\left(\frac{D_V}{D_{V_{70}}}\right)_{min_p} = \left\{\left(\frac{\mu\lambda)_{70}}{\mu\lambda}\right)_V^{3/4}\left(\frac{N_{V_{70}}}{N_V}\right)^2\right\}^{4/19} \qquad (2\text{-}23)$$

These results are shown in Figures 2-9 and 2-10. Due to the fact that in the temperature range being considered the vapor transport factor increases as the temperature is increased, the minimum diameter of the vapor transport section decreases with increasing temperature. Similarly because of the inverse relationship that exists, the magnitude of $r_p \cos\theta$ decreases with increasing temperature in the range of operation that was analyzed.

2. Sonic Vapor Limitation

In most conventional applications the maximum heat transport capability is determined by the capillary pumping limit. However, in a capillary pumped loop where the diameter of the vapor transport section will be rather small the sonic vapor flow limitation must also be considered. For the case of uniform heat input at the evaporator section the maximum heat which can be transported without being limited by gasdynamic choking is given by[5]

$$q_{max} = \sqrt{\frac{k\,R_V\,T_V}{2\,(k+1)}}\,(\rho\,A)_{V_{CH}}\,\lambda \qquad (2\text{-}24)$$

where A_V is the cross-sectional area of the vapor flow in the transport section

$$A_V = \frac{\pi}{4}\,D_{V_{CH}}^2 \qquad (2\text{-}25)$$

FIGURE 2-9

EFFECT OF TEMPERATURE ON REQUIRED PORE SIZE

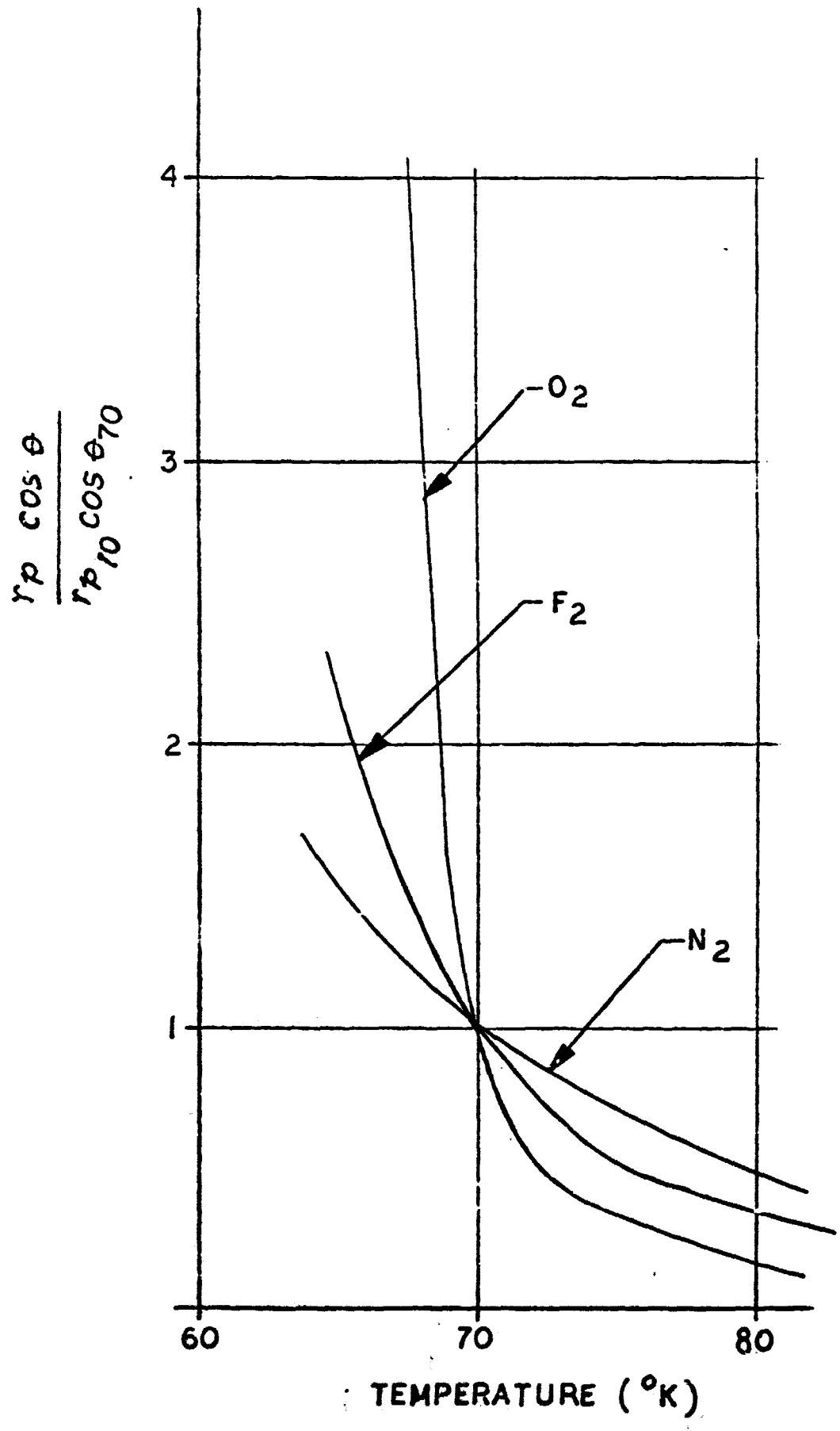

FIGURE 2-10

EFFECT OF TEMPERATURE ON THE DIAMETER OF THE VAPOR TRANSPORT SECTION (CAPILLARY PUMPING LIMIT)

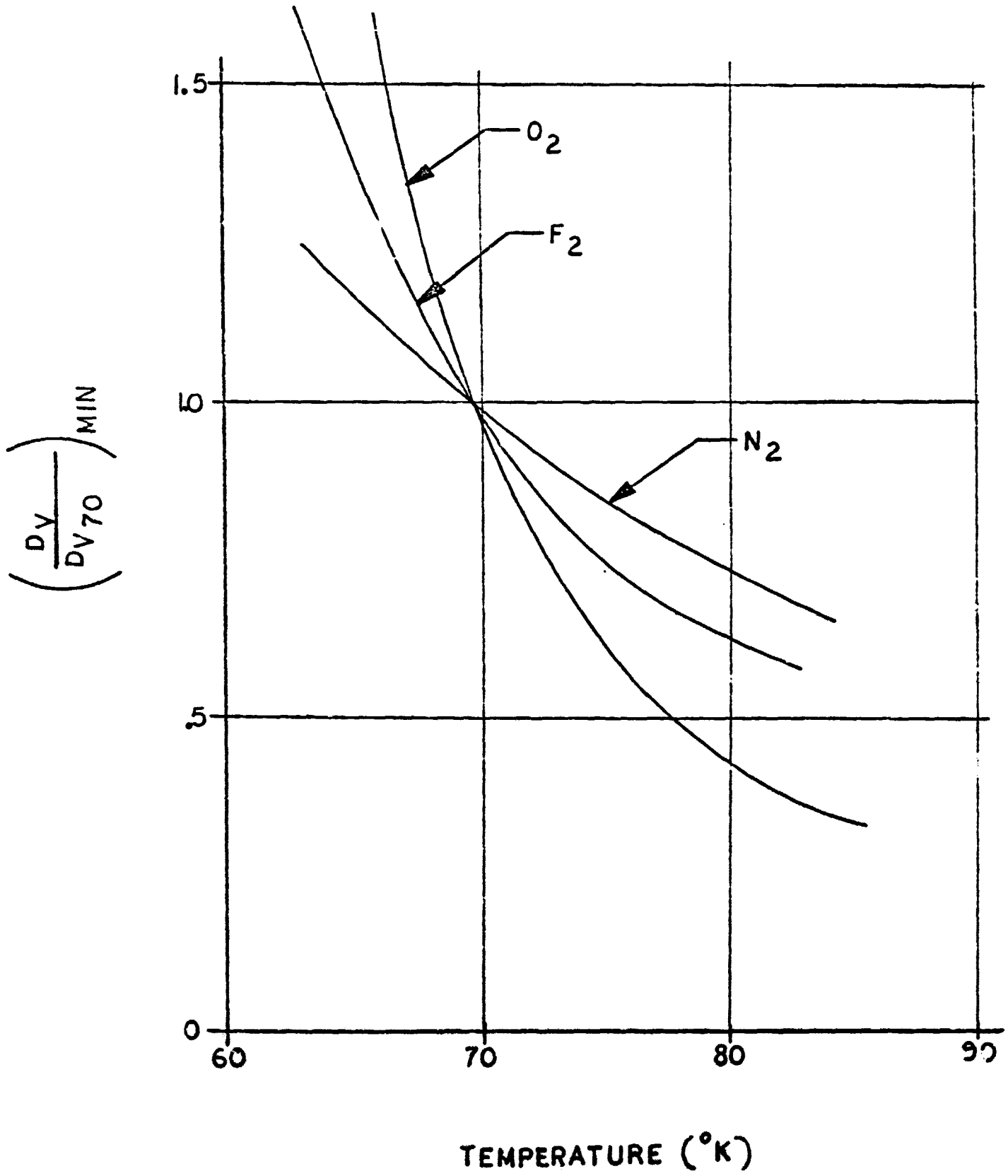

The maximum heat that can be transported subject to the sonic vapor limitation is shown in Figure 2-11 as a function of the diameter of the transport section for a given vapor temperature ($T = 70^{o}K$) for nitrogen, oxygen and fluorine. As indicated in this Figure, the sonic vapor limitation is especially prohibitive for oxygen. This is due to the fact that oxygen's vapor density is much smaller than that of either nitrogen or fluorine.

The effect of different operating temperatures on the minimum allowable vapor flow diameter for a given maximum heat transport requirement is readily determined by combining Eqs. (2-24) and (2-25). Thus

$$D_{V_{CH}} = \left(\frac{2\,(k+1)}{k\,R_V\,T_V}\right)^{1/4} \left(\frac{4}{\pi}\,\frac{q_{max}}{\rho_V\,\lambda}\right)^{1/2} \tag{2-26}$$

or

$$\left(\frac{D_V}{D_{V_{70}}}\right)_{CH} = 2.9 \left(\frac{(\rho_V\,\lambda)_{70}}{\rho_V\,\lambda\sqrt{T_V}}\right)^{1/2} \tag{2-27}$$

The above ratio is shown as a function of temperature in Figure 2-12 for each of the three fluids. For a given operating temperature and heat load, Figures 2-11 and 2-12 allow one to determine the minimum diameter of the vapor transport section that can be used without incurring gasdynamic choking. Ideally, in order to reduce the system weight as well as the heat leaks, the diameter of the transport sections should be as small as possible within the limits as dictated by performance requirements and practicality. As indicated in Figure 2-12 the minimum allowable diameter associated with the sonic vapor limitation decreases with increasing temperature. This variation is due primarily to the change in the vapor density with changes in temperature and is greatest for oxygen and smallest for nitrogen.

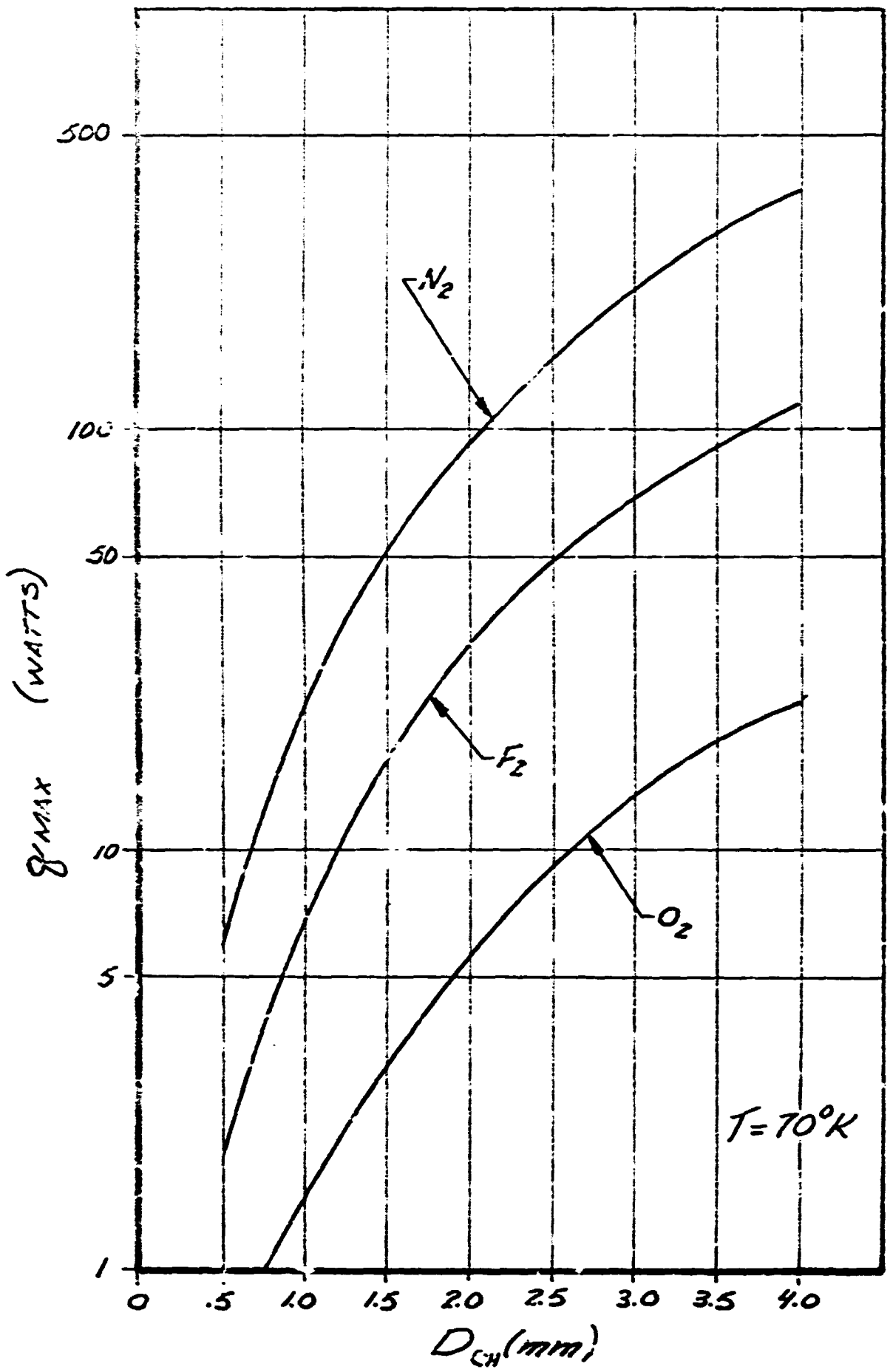

FIGURE 2-11 MAXIMUM HEAT TRANSPORT ASSOCIATED WITH SONIC VAPOR LIMITATION

FIGURE 2-12

EFFECT OF TEMPERATURE ON THE DIAMETER OF THE VAPOR TRANSPORT SECTION(SONIC VAPOR LIMIT)

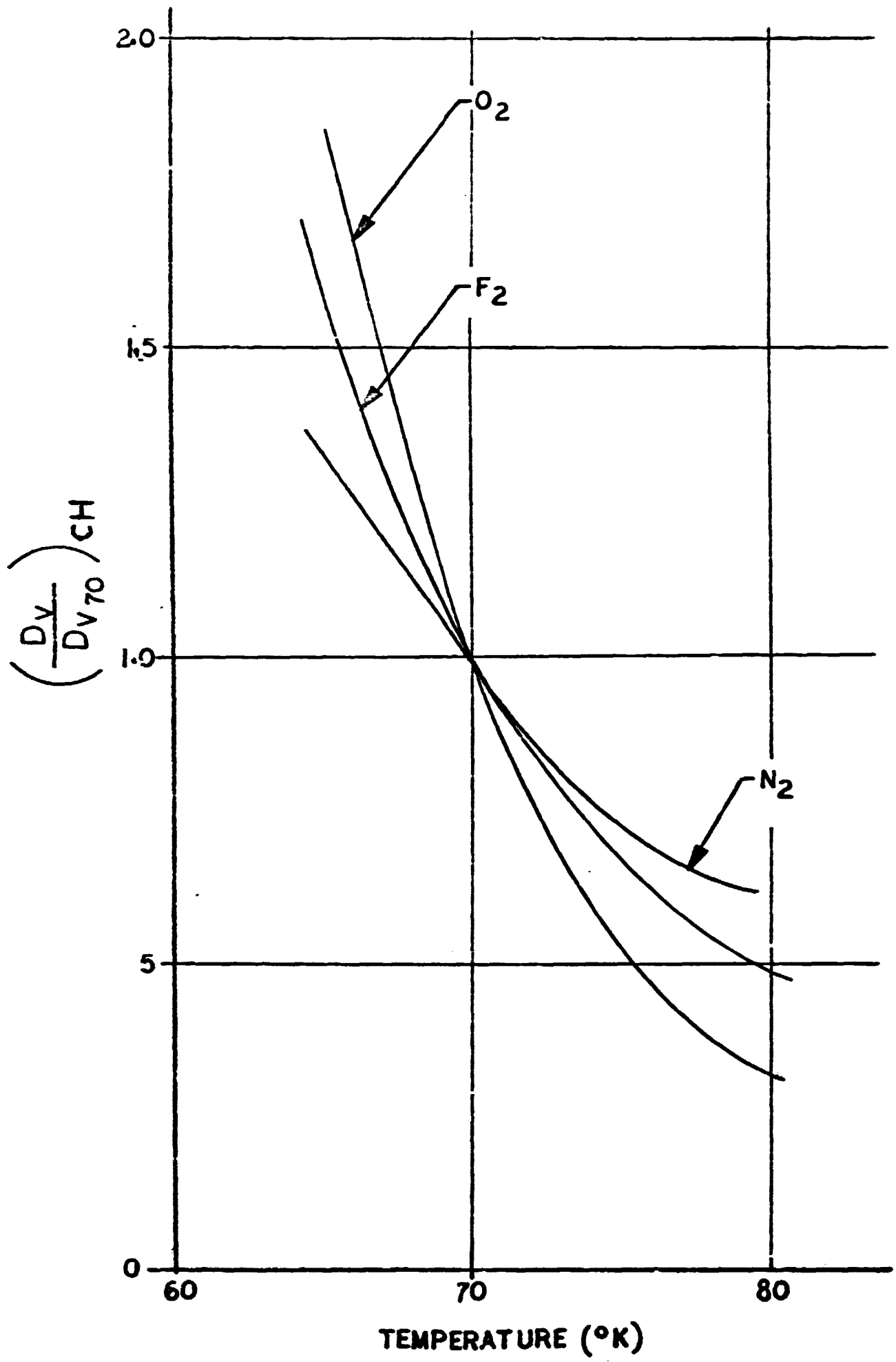

For a given heat transport requirement, the design of the capillary pumped loop will be based on the larger of the two diameters as dictated by either the sonic vapor or capillary pumping limitation.

Section 3

EVALUATION OF THE NON-WETTABILITY OF CRYOGENIC LIQUID-SOLID COMBINATIONS

The analytic evaluation of a non-wetting cryogenic heat pipe system showed that this concept is feasible even for very low non-wetting contact angles. As a result a comprehensive literature survey was performed to determine whether non-wetting cryogenic liquid/solid combinations are feasible and if so which combinations have the greatest potential. Results of the survey established that contact angles greater than ninety degrees are possible with cryogenic fluids provided that the critical surface tension of the solid surface is less than half the liquid surface tension. Because of the relatively low surface tensions of cryogenic liquids only those solid surfaces which are generally classified as low energy surfaces qualify. Test samples were made containing the most promising low energy surfaces and the contact angles of liquid nitrogen oxygen, and Freon 13 on these surfaces were measured in a cryogenic dewar system using the "tilting plate" method. The cryogenic contact angle measurements and the results of the literature survey are discussed in detail in the following sections.

A. Literature Survey

A literature survey was conducted to obtain information pertaining to the relationship between wettability and the structure of solids and liquids, in order to establish guidelines for the selection of potential "non-wetting" cryogenic materials. Methods for the measurement of contact angles were also examined.

The basic expression for the contact angle was developed by Young[6] in terms of the surface tensions of the liquid/vapor (σ_{lv}), solid/vapor (σ_{sv}), and solid/liquid (σ_{sl}) interfaces (refer to Figure 3-1) and is

$$\sigma_{sv} = \sigma_{sl} + \sigma_{lv} \cos \theta \qquad (3\text{-}1)$$

These surface tensions are actually the average free energy per unit area of the interfaces. It is experimentally feasible to measure σ_{lv} but extremely difficult to measure σ_{sv} and σ_{sl}.

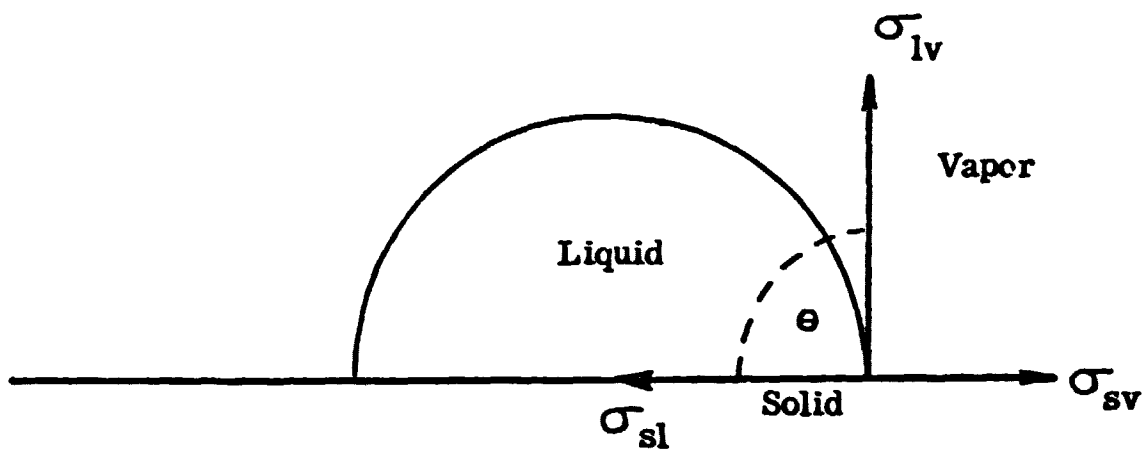

FIGURE 3-1. CONTACT ANGLE
BETWEEN A LIQUID AND A SOLID SURFACE

Dupre[7] introduced the work of adhesion of liquid and solid:

$$W_A = \sigma_{sv} + \sigma_{lv} - \sigma_{sl} \qquad (3\text{-}2)$$

The combination of these two equations yields

$$W_A = \sigma_{lv} (1 + \cos \theta) \qquad (3\text{-}3)$$

Not until quite recently was it recognized that the adsorption of vapor on the solid surface could affect the contact angle.[8] When this phenomena is included the Young and Dupre Equations can be written more appropriately as:

$$\sigma_{sv^o} = \sigma_{sl} + \sigma_{lv^o} \cos \theta \qquad (3\text{-}4)$$

$$W_A = \sigma_{s^o} + \sigma_{lv^o} - \sigma_{sl} \qquad (3\text{-}5)$$

where the subscripts have the meaning:

sv^o = solid in contact with only saturated vapor

lv^o = liquid in contact with only saturated vapor

s^o = solid in vacuum

and then

$$W_A = (\sigma_s{}^o - \sigma_{sv}{}^o) + \sigma_{lv}{}^o \ (1 + \cos \theta) \qquad (3\text{-}6)$$

The first term in parentheses, which represents the decrease in free energy on immersion of the solid in the saturated vapor phase is always positive and has generally been ignored by most authors. The surface tension of a liquid in air is very nearly identical to that in vacuum (i.e., $\sigma_{lv} \simeq \sigma_{lv}{}^o$) whereas there is a more marked difference for the solid's surface tension. Consequently, with these factors in mind, comparison of Eqs. (3-3) and (3-6) indicates that the presence of the vapor film will tend to increase the contact angle.

The non-reproducibility of contact angles has been a major problem area for many years. One important factor in this has been shown to be surface roughness. Wenzel[9] defined a roughness factor "r" as the ratio between the true area of the solid and the apparent area. He then derived the relation

$$r = \frac{\cos \theta'}{\cos \theta} \qquad (3\text{-}7)$$

with θ = true contact angle

θ' = measured contact angle

From this, it can be seen that, when the actual contact angle is less than 90^o, the measured angle will almost invariably be smaller since a perfectly smooth surface is essentially unattainable and the roughness factor will always be greater than unity. Also, when

the actual angle is greater than 90^{o}, the measured angle will be larger than θ. Thus, any small irregularities in the surface will accentuate the "non-wetting" appearance, rather than possibly masking it out. Note, however, that this effect only makes the observation of "non-wetting" materials more positive; it does not change the actual wettability of the material.

There has also been quite a bit of controversy over the significance of the differences between advancing and receding contact angles. Recent work[10] has indicated that using scrupulously clean surfaces and liquids will yield identical results in both directions except in the case where the liquid molecules can penetrate the surface, thereby changing its characteristics. Among the liquids normally studied, water is nearly unique in this respect. However, the molecular size of some of the more common cryogens (e.g., nitrogen and oxygen) is only slightly larger than that of water and surface penetration by these cryogenic liquids is a potential problem. As discussed later, testing was conducted with Freon 13, which has relatively large molecules, to determine whether surface penetration was a problem with either nitrogen or oxygen.

There are also liquids that can deposit a monolayer upon the surface in such a manner as to present a new surface to the bulk liquid. This new surface is then able to prevent further wetting. These materials are termed "autophobic". This effect is the basis of the retraction method of monolayer preparations discussed in a later section.

Zisman and his co-workers[11] have shown that, for many homologous series of liquids, $\cos\theta$ increases linearly for a given surface with decreasing σ_{lv} of the liquid. They then define a critical surface tension for wetting (σ_c) as the intercept of the horizontal line, $\cos\theta = 1$, with the extrapolated straight line plot of $\cos\theta$ vs σ_{lv} (Cf. Figure 3-2). Even non-homologous series of liquids fall in narrow rectilinear

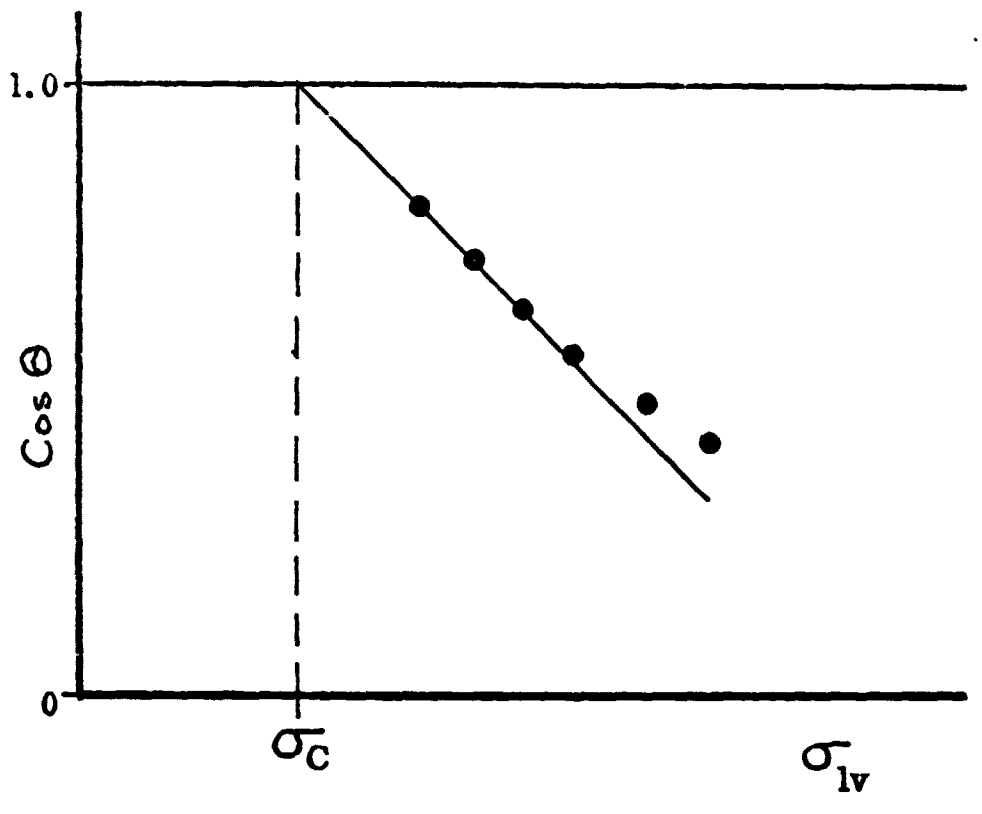

FIGURE 3-2. DETERMINATION OF CRITICAL SURFACE TENSION (σ_c) FROM A HOMOLOGOUS SERIES OF LIQUIDS

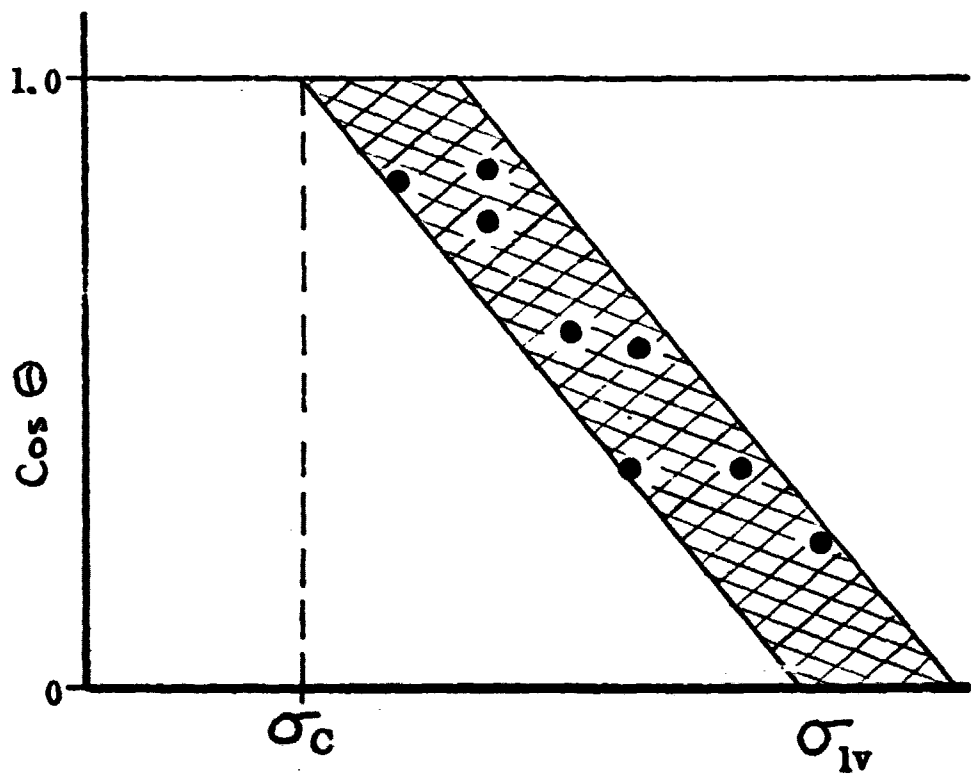

FIGURE 3-3. DETERMINATION OF CRITICAL SURFACE TENSION (σ_c) FROM A NON-HOMOLOGOUS SERIES OF LIQUIDS

bands on this type of plot for a given surface (Cf. Figure 3-3). In such a plot, the lower intercept of the band is chosen as σ_c. This value is more generally characteristic of the solid and behaves relatively as one would expect σ_{so}, the specific surface free energy of the solid. The critical surface tension of the solid is important in the present work, since it has been shown that for non-wetting the minimum value of $(\sigma_{lv} - \sigma_c)$ must be more than one-half the surface tension of the liquid,[12] or

$$\sigma_c < 0.5\,\sigma_{lv} \qquad (3\text{-}8)$$

There is still quite a bit of discussion regarding the appropriateness of the various terms and relationships involved here. The "accepted" meaning of non-spreading is $\theta \neq 0^o$. If the liquid wets the solid completely at a rate depending only on the viscosity of the liquid and the roughness of the surface then we say $\theta = 0^o$. If $\theta \geq 90^o$, then the liquid will tend to be repelled by a solid surface. In the present report, this last effect is referred to as "non-wetting."

For the liquids commonly studied at room temperature (water, hydrocarbons, alcohols, organic salt, etc.) surfaces have been found to increase their non-wetting characteristics in the order of metals, soft organic solids (e.g., paraffins), polymers and long chain monolayers. Only the polymers and monolayers exhibit very low σ_c. The lowest known value of σ_c is for a monolayer of a perfluorocarboxylic acid, and this is 5.6 ergs/cm^2.[13] Critical surface tensions of various low energy surfaces are listed in Table 3-1. These results indicate that the surfaces most likely to exhibit non-wetting are highly fluorinated monolayers and polymers. The wettability of such surfaces increases with the type of atom attached to the outer carbon atoms in the order: F, H, Cl, O, N.[22] In general, the most non-wetting monolayers consist of long chain,

TABLE 3-1

CRITICAL SURFACE TENSIONS OF SOME LOW ENERGY SURFACES

		σ_c (Ergs/cm^2 at 20°C)	Reference
A.	Coated Surfaces		
	$-CF_3$	6	13
	$-CF_2H$	15	14
	$-CF_3$ and $-CF_2-$	17	15
	$-CF_2-$	18	16
	$-CH_2-CF_3$	20	17
	$-CH_3$ (crystal)	22	18
	$-CH_3$ (monolayer)	24	19
B.	Polymers		
	Polymethacrylic ester of θ' -octanol	10.6	20
	Polytetrafluoroethylene	18.5	16
	Polyethylene	31	18
	Polyvinyl chloride	39	21
	Polyvinylidene chloride	40	21

linear, dipolar, organic molecules. The best of these are close-packed vertically so that the new surface presented to the fluid consists essentially of the terminal groups of these molecules (Cf. Figure 3-4).

Zisman[11] has shown that for a given surface and liquid the effect of temperature on the contact angle is given by

$$\cos \theta = a + b\,T \qquad (3\text{-}9)$$

where a and b are constants associated with the particular liquid and solid surface. The constant b is always positive and thus as a general rule the contact angle for a given liquid/solid combination will increase as the temperature of the system decreases. Equation (3-9) is based on the fact that in general the liquid surface tension decreases almost linearly with increasing temperature and on experimental results similar to those shown in Figures 3-2 and 3-3. This relationship assumes that the critical surface tension is essentially independent of temperature and is valid over small temperature ranges.

The liquid surface tensions of potential cryogenic working fluids (e.g., nitrogen, oxygen, fluorine, etc.) vary between 6 and 18 dynes/cm in the temperature regime of interest (70-90°K). Consequently, of the surfaces listed in Table 3-1, only the perfluorodecanoic monolayer would be potentially non-wetting based on the room temperature criterion (Eq. 3-8). However, this criterion is not exact and furthermore may not be applicable at cryogenic temperatures. Since no data is available regarding the variation of the critical surface tension with temperature, it is also possible that σ_c is substantially lower at cryogenic temperatures. As a result, since the literature search did not discount the feasibility of obtaining a non-wetting cryogenic liquid/solid combination, a basic experimental study was undertaken. The purpose of this research was to measure the contact angles of various cryogenic liquids on different low-energy surfaces.

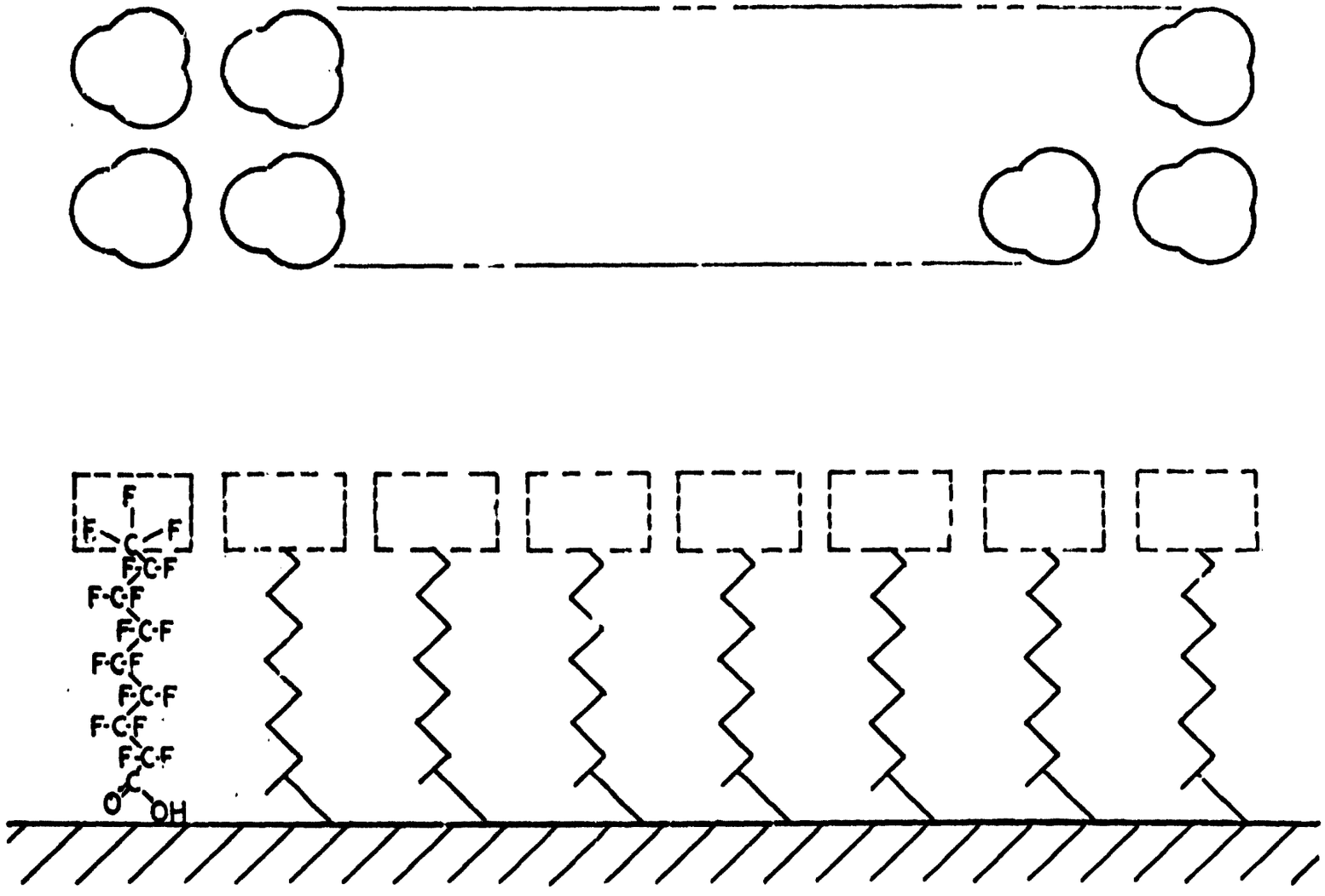

FIGURE 3-4. SCHEMATIC OF ORGANIC - (CF_3) MONOLAYERS

B. Preparation of Low Energy Surfaces

The various low energy surfaces selected for cryogenic contact angle measurements included the perfluoro-decanoic and octanoic monolayers and also Teflon and polyethylene. In addition to these, a barrier coating (FC-706) and a chromium complex (L-1632) which were recommended because they have low critical surface tensions (~15 dynes/cm) were also investigated. The monolayers and coatings were applied to different metallic substrates which included aluminum, copper, and 304 stainless steel. The monolayers were formed by immersing a previously cleaned metal plate in a solution of the perfluoro-acid and n-decane solvent (~10^{-4} molar concentration) for one hour and then slowly withdrawing the sample vertically. Approximate overall dimensions for each of the test samples were 2.5 cm x 1.25 cm x 0.125 cm.

One outstanding fact emphasized in the literature is that meaningful contact angle measurements require extremely clean and smooth surfaces. Many of the reported variations are directly attributable to surface roughness or inadequate safeguards against minute amounts of contaminants. Therefore, rather stringent cleaning and handling procedures were established for the test samples.

The metal substrates were emery buffed and lapped to the desired thickness. Any scratches were removed with crocus cloth and the samples were then polished with a buffing wheel and jeweler's rouge to a surface finish of approximately 4. The substrates were then cleaned with hot trichloroethylene, methanol, and "Sparkleen", and finally rinsed three times in hot triple-distilled water. After cleaning, each substrate was tested for cleanliness by the "sessile drop" method* with distilled water.

---

*This is the most common method of contact angle measurement and consists of placing a drop of the test liquid on the test surface and slowly adding more liquid to the drop until no further change in the contact angle is observed. The contact angle can be measured directly as indicated in Figure 3-1 or calculated in various ways from measurements of the height and the radius of the drop.

If a contact angle of less than 15° was observed, the substrate was considered clean. Cleaned substrates were then heated by a flame on the side opposite the test surface until the appearance of a slight discoloration was noted. The metal was then immersed while it was still hot (150-175°C) into one of the perfluoroacid solutions or coatings for one hour. Withdrawal of the samples was done at a rate of approximately 5 millimeters per minute. This slow rate was used to insure that a uniform monolayer was formed. Samples coated with the chromium complex were cured at 100°C in an oven for five minutes after they were withdrawn from the solution.

The Teflon and polyethylene surfaces were abraded with #400 emery paper to remove gross scratches and then cleaned with methanol in an ultrasonic tank. A smooth glassy surface was then obtained by pressing these samples between two clean microscopic slides at approximately 500 psi and 150°C for a minimum of three hours. These surfaces were given a final cleaning in boiling nitric-sulfuric acid (1:2) for 15 minutes and then rinsed in triple-distilled water. The samples were generally dry when removed from the water.

Once a sample had been prepared its contact angle with water was measured by the "sessile drop" method. If the contact angle was approximately equal to or greater than the literature value, the sample was accepted for the cryogenic tests. This acceptance criteria was based on the premise that in order for a sample to be non-wetting with a cryogen it should exhibit a high degree of non-wettability with water which has a significantly higher liquid surface tension. In general, the contact angles of water on the low energy surfaces that were accepted were approximately 100° or greater. Prior to their insertion in the cryogenic test system the test samples were stored in a vacuum desiccator or inert atmosphere.

C. Cryogenic Contact Angle Measurements

Contact angles were measured at several temperatures for each of the three cryogenic liquids--nitrogen, oxygen, and Freon-13--on the various low energy surfaces previously discussed. Aluminum and platinum metal were tested as representative high energy surfaces.

1. Test System

Several of the methods which exist for measuring contact angles are the sessile drop, tilting plate, porous plug, and wetting balance techniques, etc. The tilting plate method had been selected for the cryogenic tests because it appeared to be the only practical technique for contact angle measurements with cryogenic liquids. This technique is shown schematically in Figure 3-5. It is rather straightforward in that a plate several centimeters wide is dipped into the test liquid and rotated until the liquid level remains perfectly horizontal up to the surface of the plate. For this condition the inclination of the plate relative to the liquid surface is the contact angle. This technique is one of the most accurate and gives good reproducibility.

The dewar and sample holder that were used to perform the cryogenic contact angle tests are shown in Figure 3-6. A schematic of the dewar is given in Figure 3-7. Basically it consists of a 7.5 cm cylindrical inner test chamber with two 2.5 cm circular viewing ports located 180^{o} apart. The inner set of windows are sapphire for corrosion resistance. The outer set of windows are optical quartz. A cooling coil and resistance heater are wrapped around the outside of the test chamber to provide cooling and temperature control. The well surrounding the inner chamber contains evacuated super insulation.

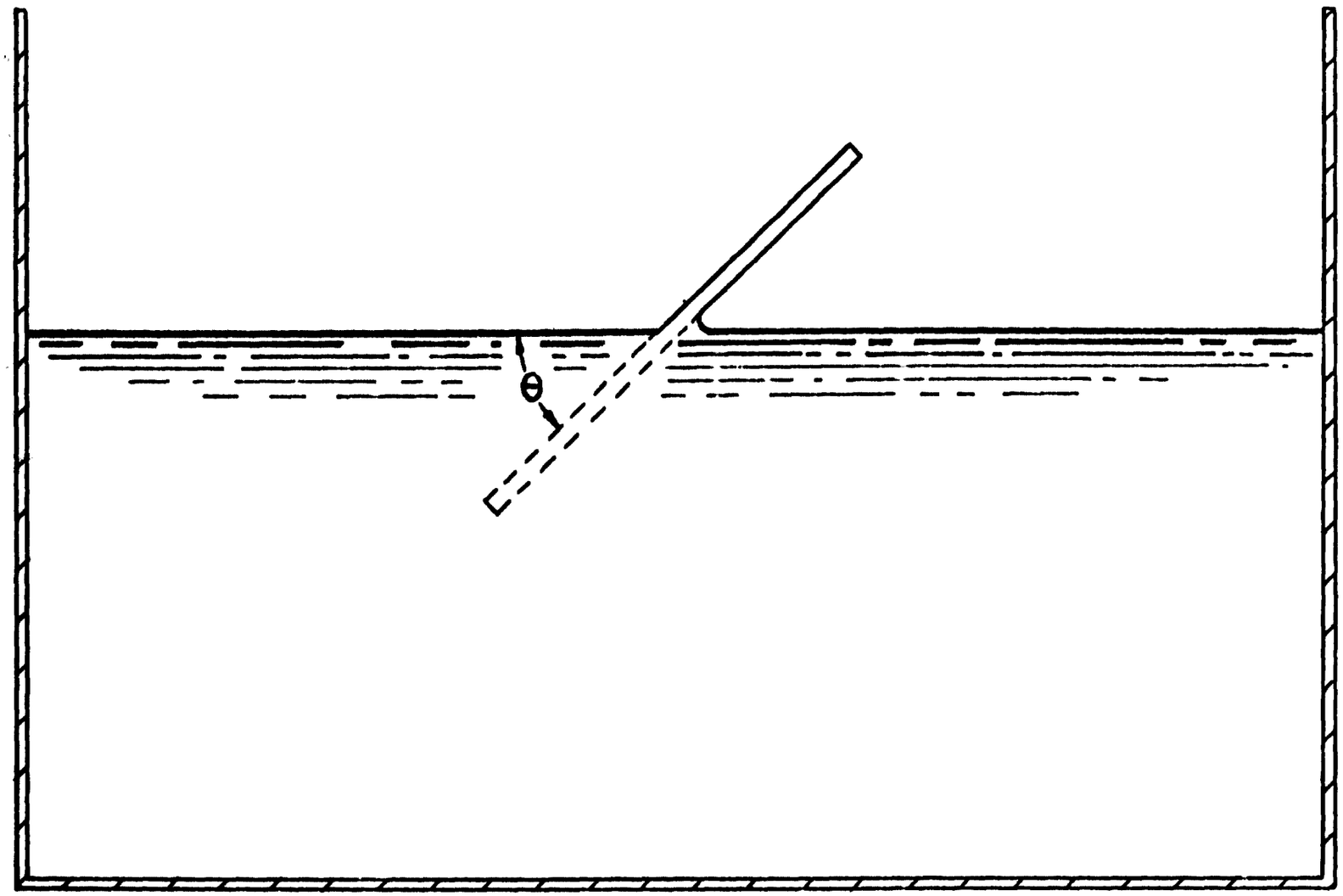

FIGURE 3-5. SCHEMATIC OF TILTING PLATE METHOD FOR CONTACT ANGLE MEASUREMENT

FIGURE 3-6

DEWAR AND SAMPLE HOLDER FOR
CRYOGENIC CONTACT ANGLE TESTS

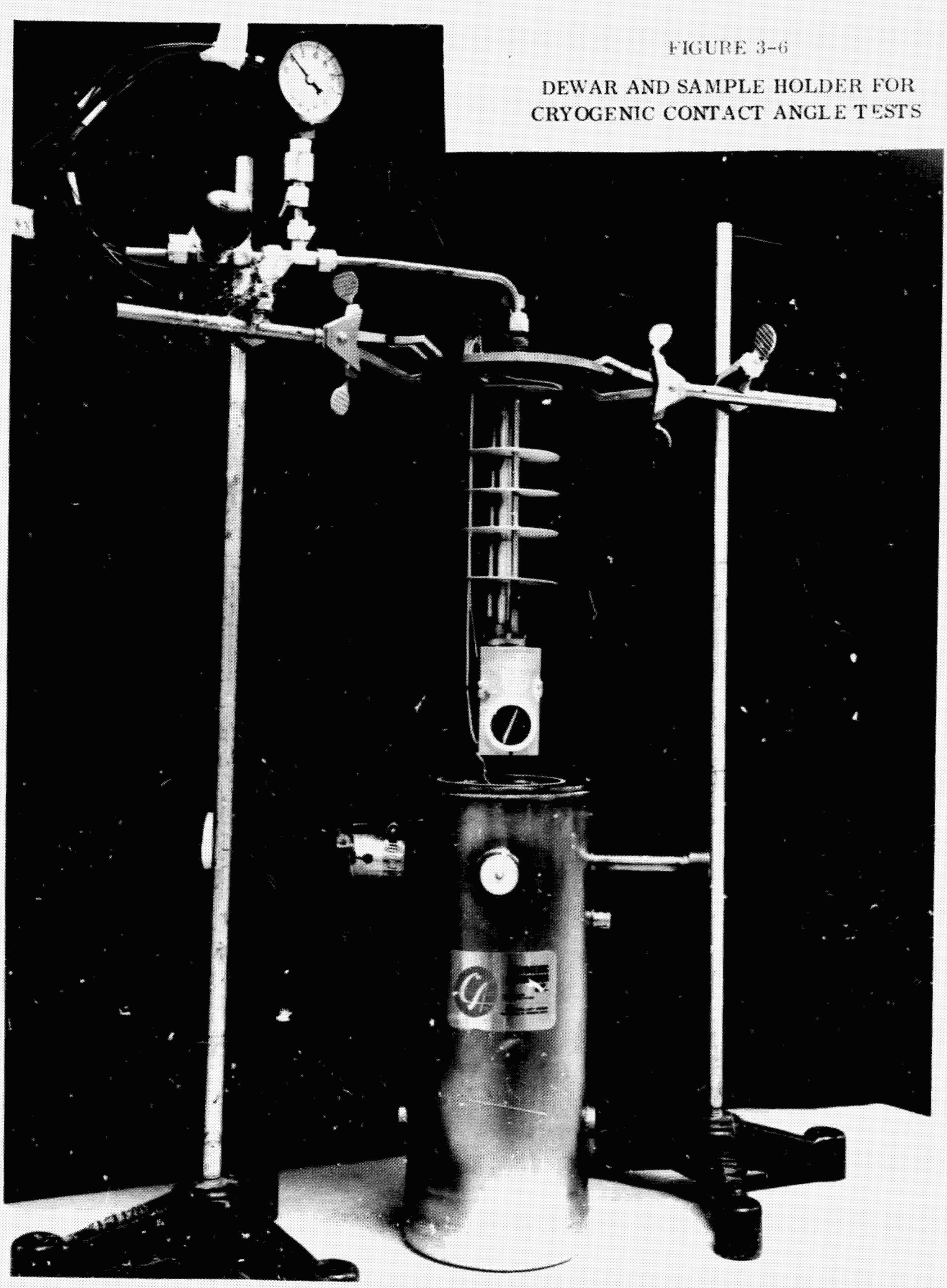

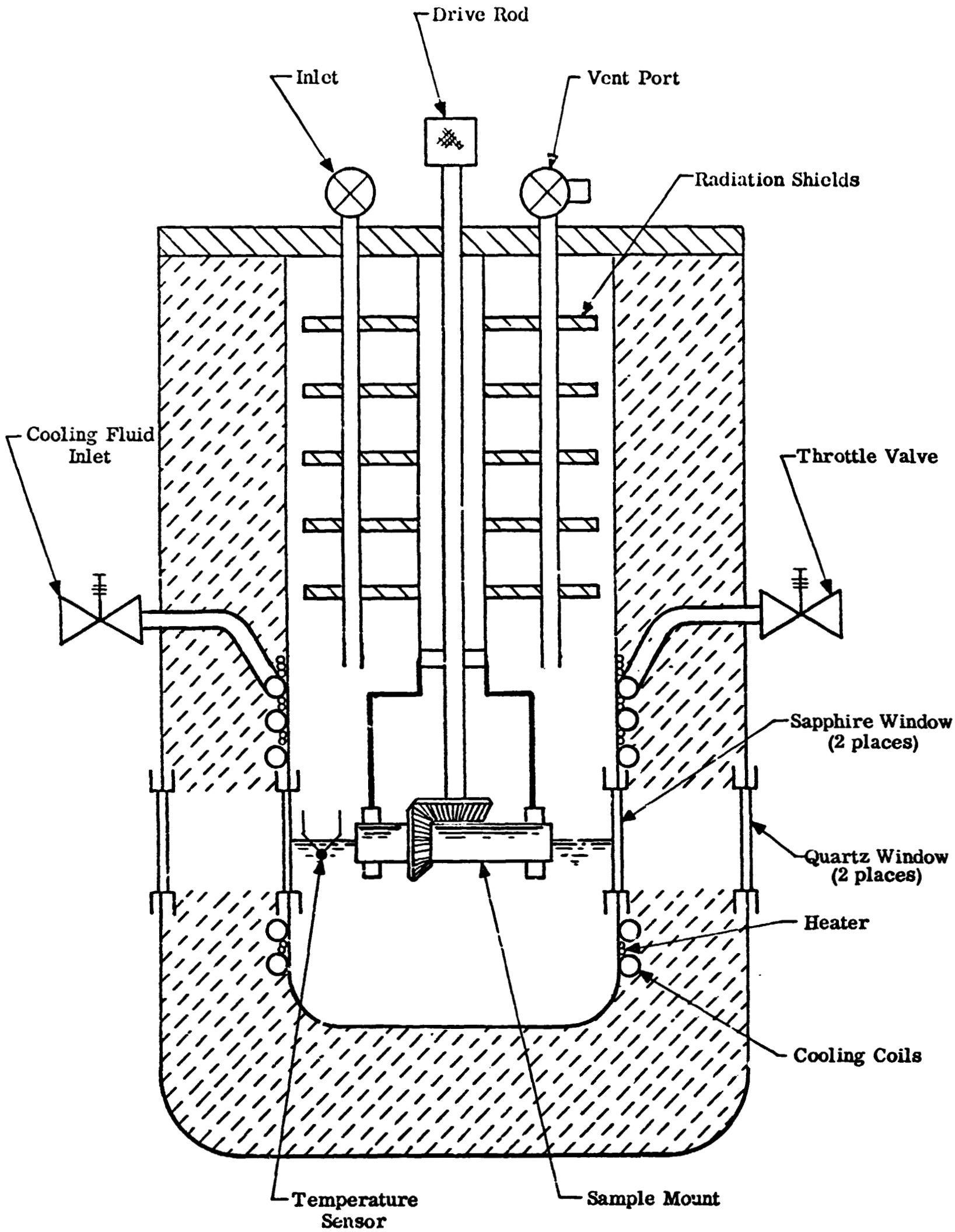

FIGURE 3-7. CRYOGENIC DEWAR FOR CONTACT ANGLE MEASUREMENTS

The sample mount consists of an internally slotted cylinder 4.5 cm long by 2.3 cm internal diameter. Samples are held in the slots by copper wedges. Rotation of the cylinder is accomplished by means of a bevel gear set and drive rod. The drive rod extends through the top of the dewar and is aligned with a protractor on the dewar lid. A set of aluminum radiation shields are located above the sample holder to reduce the heat losses. Three chromel-alumel thermocouples are located to read the temperatures at the inside surface of the brass lid, at the top of the sample holder above the cryogen level, and at the bottom of the sample holder in the liquid cryogen.

During testing the dewar system was suspended from a wall bracket within a temporarily enclosed clean room as shown in Figure 3-8. The bracket was mounted to the wall through four neoprene rubber blocks and the support fixture was attached to the bracket through four more neoprene rubber blocks in order to minimize vibrations in the cryogenic liquid surface during the tests. The dewar was mounted to the support by means of three rods which are extensions of the lid bolts on the dewar. These rods were bolted through an aluminum ring at their upper ends. Three leveling screws were used to support this ring on ball bearings mounted in V-slots such that the observation windows on the dewar are reproducibly aligned with respect to a fixed optical axis.

A schematic of the optical system which was used to determine the cryogenic contact angles is shown in Figure 3-9. This system is based on Ablett's experiment.[23] Basically it consists of a light source and slit, a condenser lens, an objective lens, and a screen mounted on two optical

FIGURE 3-8

CRYOGENIC CONTACT ANGLE TEST SYSTEM

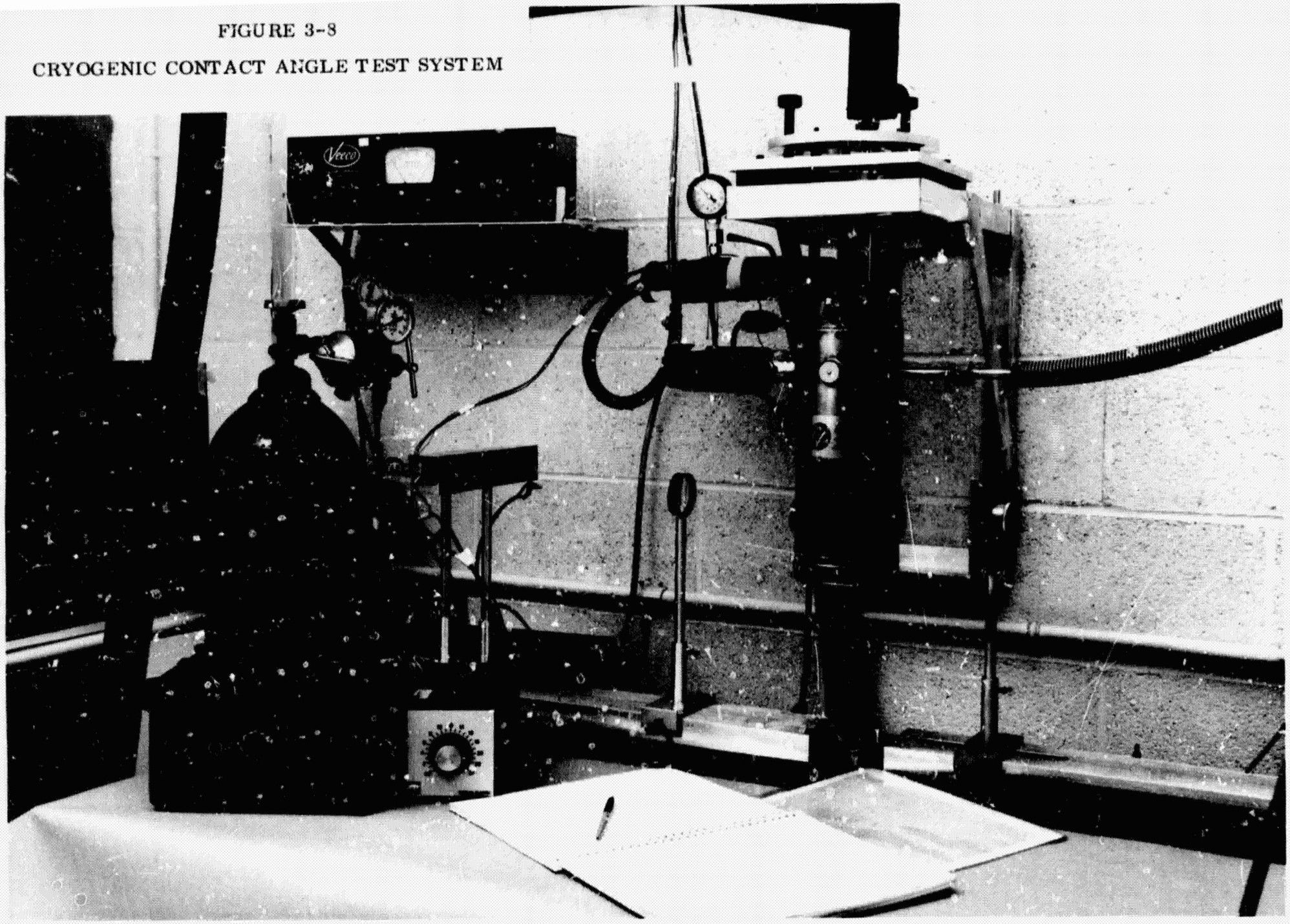

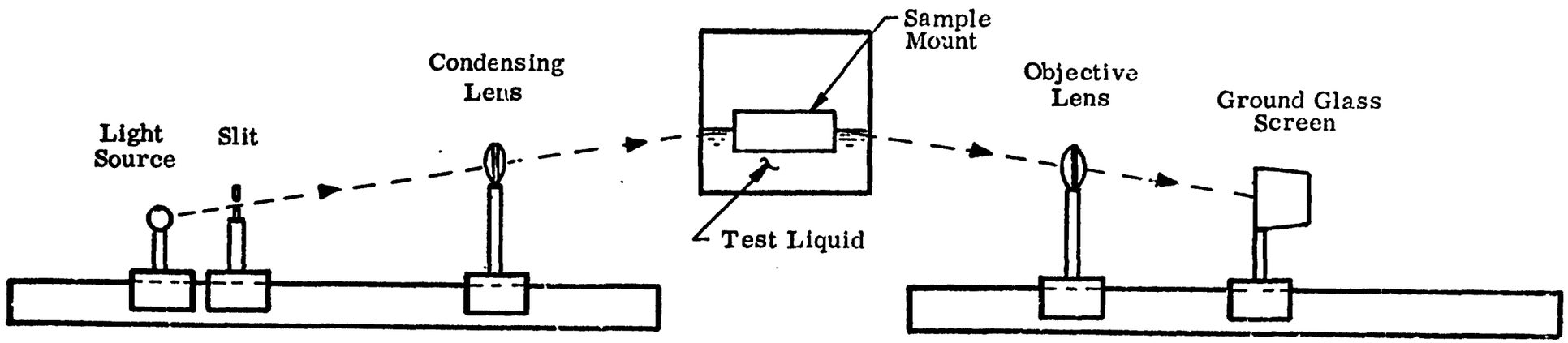

FIGURE 3-9. SCHEMATIC OF OPTICAL
SYSTEM FOR CONTACT ANGLE MEASUREMENTS

benches. The light source is a 6 watt, 20 cm fluorescent tube, GE-F6T5-CW which was mounted just behind a 0.2 mm x 5 cm long slit in 1.7 mm aluminum plate. The image of this slit is focused on the surface of the test liquid at approximately the center of the sample by a 12.7 cm focal length condenser lens. On the opposite side of the dewar is a 12.7 cm objective lens and a ground glass screen. This latter arrangement gives approximately a three-fold magnification of the slit image on the screen. Contact angles were determined by both direct observation using only the condenser lens and indirect observations wherein the image on the screen was used to establish when the liquid surface was horizontal at its point of intersection with the solid.

The cooling system for this experiment is shown schematically in Figure 3-10. A liquid nitrogen coolant storage dewar is connected to the cooling coil through a vacuum insulated line with a bayonet fitting. At the outlet end of the cooling coil are provisions for evacuation, inert gas purging, and venting.

The plumbing associated with the filling and evacuation of the test chamber is also shown in Figure 3-10. The test cryogen vessel is connected to the test chamber by a foam rubber insulated line and a vacuum insulated "lance" inserted into the test chamber to a point at the top of the sample holder. A valving arrangement allows the test cryogen to be vented outside until the vapor has been displaced and the liquid is freely flowing. This avoids rewarming the sample holder each time test cryogen is introduced to the chamber. The outlet tube on the test chamber also has provision for evacuation, inert gas purging and venting.

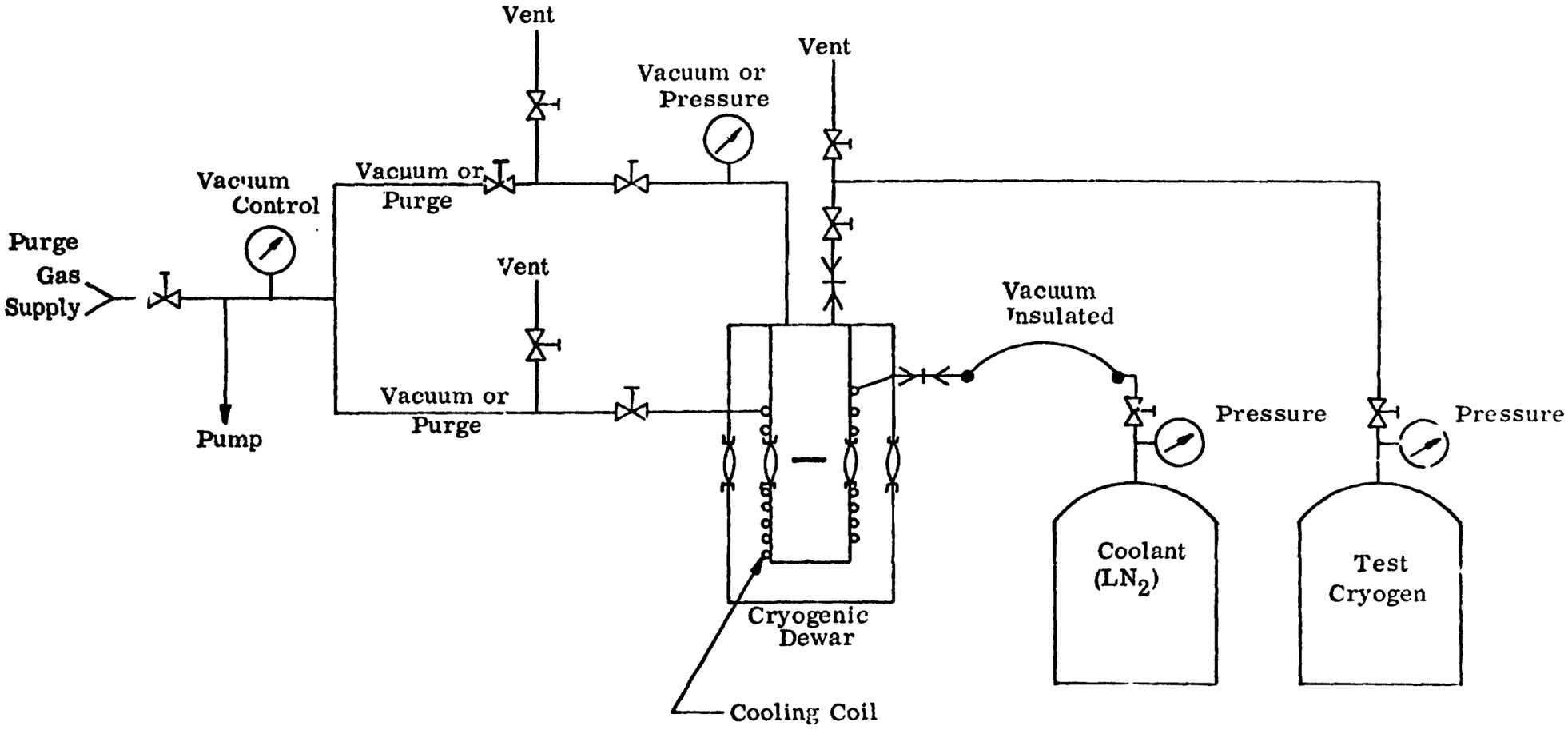

FIGURE 3-10. SCHEMATIC OF TEST SYSTEM FOR CRYOGENIC CONTACT ANGLE MEASUREMENTS

2. Test Procedure

The following is the procedure used in performing the cryogenic contact angle measurement tests:

(1) The sample surface is checked for smooth finish, cleaned, and prepared.

(2) The contact angle of the sample with water is measured by the "sessile drop" technique (1 small drop near a corner of the sample) immediately prior to insertion in the dewar test section.

(3) The inner walls of the dewar and the sample holder is held under an inert atmosphere until the sample is inserted.

(4) The sample is inserted under a flow of inert gas and the dewar reassembled.

(5) The cryogen input line is attached to the dewar, and a vacuum line is attached to the vent port and the system evacuated to $\sim 50\mu$.

(6) The coolant transfer line is attached to the dewar and the appropriate cryogenic reservoir, and the dewar is adjusted to near the desired operating temperature.

(7) The test section is filled to the appropriate level with the test liquid.

(8) The contact angle is determined by the "tilting plate" method by observation of the image on a ground glass screen and by direct observation through the objective lens.

(9) The coolant is then shut off and the dewar test section evacuated and allowed to warm to room temperature.

(10) The sample is removed under a flow of inert gas and its contact angle with water determined immediately thereafter by the "sessile drop" technique.

3. Test Results

A summary of the cryogenic contact angle measurements is given in Table 3-2. The angles given are linear averages based on at least two observations. Both the liquid nitrogen and the liquid oxygen wet all the surfaces and, as indicated in Figure 3-11, show no definite contact angle variation with temperature. The Freon 13 was also wetting; but, as shown in Figure 3-12 and discussed later, a slight increase in contact angle with increasing temperature was observed. Contact angles of these fluids on the various low energy surfaces ranged from 2.5° to 30°. The highest angle was observed for liquid nitrogen on a perfluorodecanoic monolayer. Average contact angles on clean aluminum and platinum samples were 8° and 2°, respectively.

The low angles obtained with nitrogen and oxygen on the low energy surfaces were at first thought to be due to an effect analogous to what has been observed at room temperature with water and certain surfaces. These surfaces are characterized by having a molecular free volume which is large enough to permit penetration by the water molecules. Contact angles of water on such surfaces were lower than for some organic liquids with substantially lower surface tensions. Zisman argues that, because of the very small relative size of the water molecules, they penetrate between the outer molecules of

TABLE 3-2

AVERAGE CRYOGENIC CONTACT ANGLE MEASUREMENTS

Surface	Nitrogen Temp (°K)	Nitrogen Contact Angle	Oxygen Temp (°K)	Oxygen Contact Angle	Freon 13 Temp (°K)	Freon 13 Contact Angle
Teflon	77	7.5	80.8	5.5	143	12.5
		10.0	93.5	5.0	154	10.5
		15.0	94.5	7.0	190	20.5
		16.0				
		19.0				
	79.5	10.5				
		10.5				
	80	8.2				
	81	12.0				
	95	7.5				
Perfluorodecanoic Acid (Aluminum)	77	19.0	80.2	7.5	139	8.5
	78.5	22.5		8.0	169	13.5
		24.0	80.8	8.0	174	12
		26.0	81	12.0		
	79.5	30.0	82	9		
	93	15.0	84	10		
		15.0	89.5	8		
	96	28.0		8.5		
		28.5	90	12.5		
	99	23.0		14		
			95	10.5		
				15		
			97	2.5		
				6.5		
				11		
Perfluorodecanoic Acid (Copper)	79.5	8.5	80.8	15		
				22		
			81.2	15		
Perfluorooctanoic Acid (Stainless Steel)	79.5	6.5	81	9		
		10.5	93	13		
		12.0	97	15.5		
Perfluorooctanoic Acid (Aluminum)	79.5	9.5	79.5	13	98	9
	83	13.0	82	11.5	138	11.5
	84	14.0	98	8.5	184	15

TABLE 3-2 (cont'd)

AVERAGE CRYOGENIC CONTACT ANGLE MEASUREMENTS

	Nitrogen		Oxygen		Freon 13	
Surface	Temp (°K)	Contact Angle	Temp (°K)	Contact Angle	Temp (°K)	Contact Angle
L-1632[a] (Aluminum)	79.7	5	82.5	5.0*		
	80	8		8.5*		
				8.5*		
			90	13.0*		
				15.5*		
				17.0*		
FC-706[b] (Copper)			80.8	7.0		
			86.6	6.5		
				8.5		
			90	5.5		
Polyethylene	77	15				
	78.5	10.5				
		12.5				
		13.5				
Aluminum (Uncoated)	79.5	7				
		7.5				
		9				
Platinum (Uncoated)			80.5	1.5		
				3.0		

*Oxygen appeared to react with this surface.

[a]Chromium complex of a fluorinated resin, provided by Dr. Lazert, 3M Company.

[b]Poly 1H, 1H-pentadecafluorooctyl methacrylate, provided by Dr. W. A. Zisman, NRL.

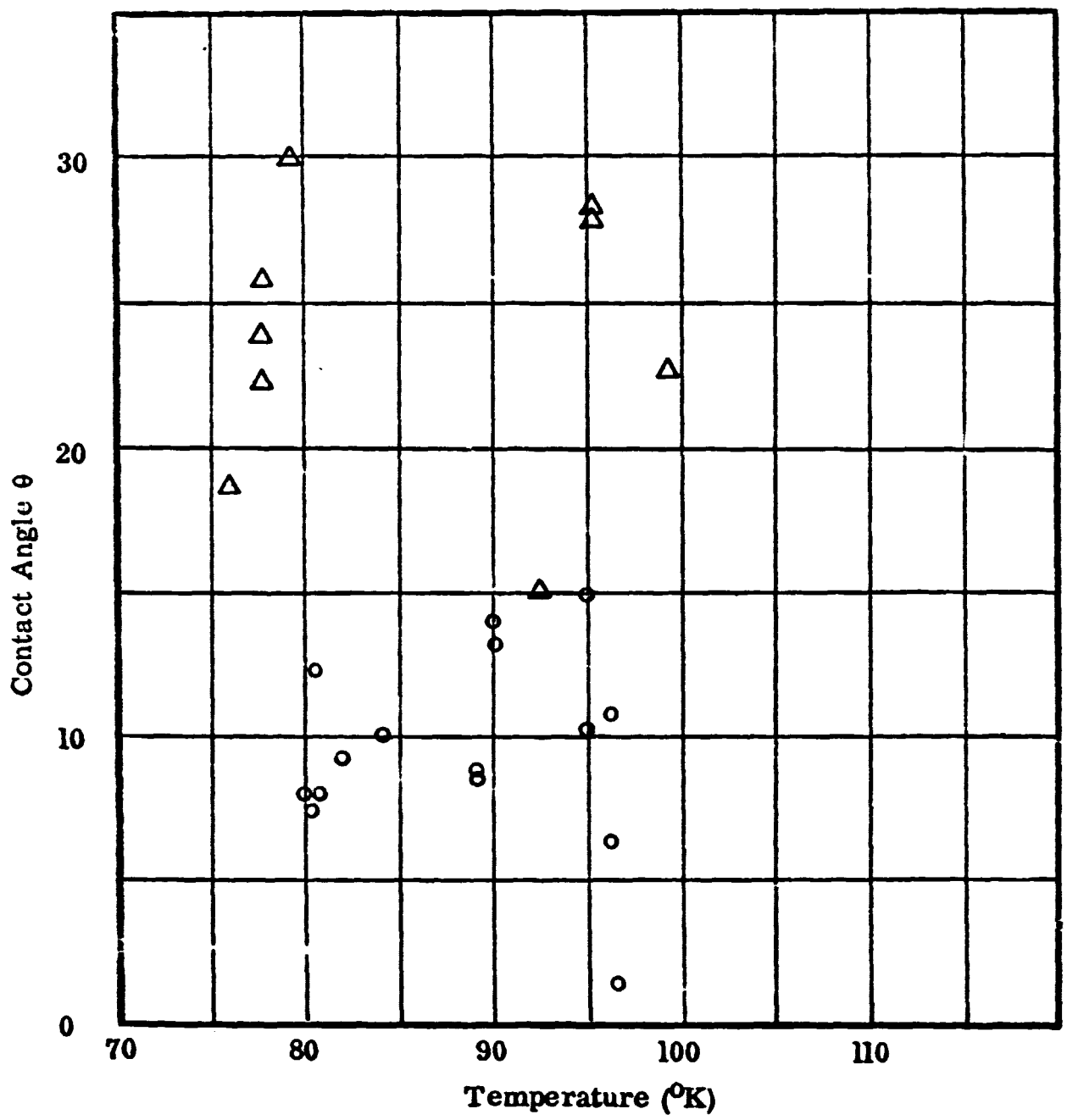

FIGURE 3-11

CONTACT ANGLE VARIATIONS WITH TEMPERATURE FOR LIQUID OXYCEN AND NITROGEN

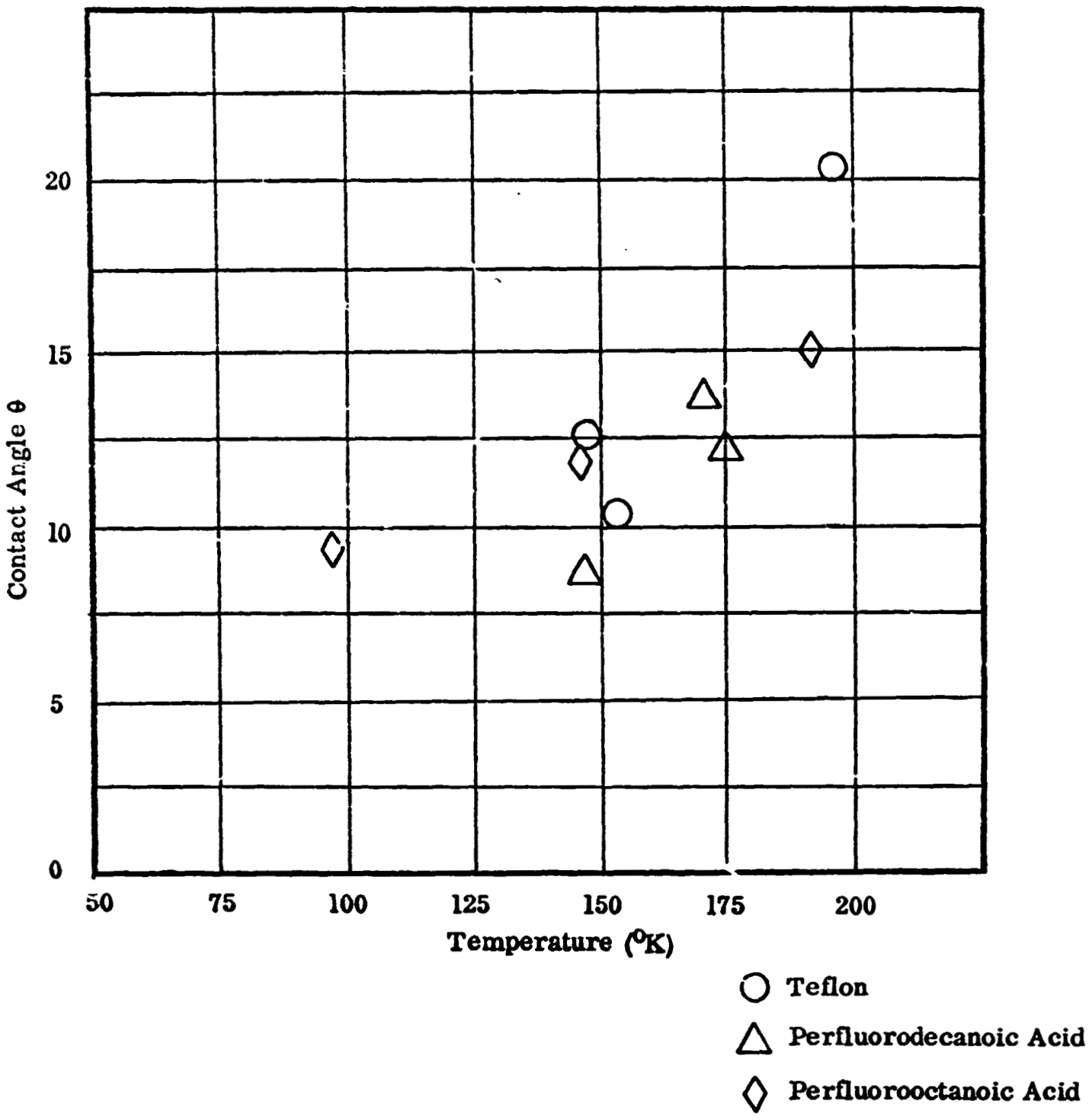

FIGURE 3-12

CONTACT ANGLE VARIATIONS WITH
TEMPERATURE FOR LIQUID FREON-13

the solid surface. Thus, a new surface (solid plus "interstitial" water) is presented to the water. This surface would then have a higher σ_c and consequently a lower contact angle with the water than would have been the case if the liquid had not peretrated the surface. This view is reinforced by the observation that dry surfaces yield higher contact angles than do the same surfaces when allowed to equilibrate with atmospheric moisture.

Freon-13 ($C\,Cl\,F_3$) was used to test this hypothesis in the present case. This molecule is substantially larger than O_2 or N_2 and approximates the size of the exposed end groups ($-C\,F_3$) in several of the test surfaces. The measured contact angles fall into the same general range as those obtained with oxygen and nitrogen, apparently discounting the possibility of this "penetration" effect.

A quite unexpected trend was observed in the measurements with Freon 13 however. This is the apparent increase of contact angle with increasing temperature, which is opposite to all previously reported observations at higher temperatures. As previously discussed the variation of contact angle with temperature based on room temperature data is given by

$$\cos\theta = a + b\,T \qquad (3\text{-}9)$$

Since the constant "b" is always positive, this relationship shows the contact angle increasing with decreasing temperature. Implicit in this equation is the assumption that the critical surface tension does not change with temperature. While the Freon 13 test data is not very extensive, it indicates that there is a possibility that Eq. (3-9) does not obtain at these lower temperatures or possibly that, at least in the cryogenic temperature regime, the σ_c increases as the temperature decreases.

If it is true that the critical surface tension has increased from its room temperature value in the cryogenic regime, this would explain why there is relatively little difference between the contact angles measured for liquid nitrogen and liquid oxygen. Oxygen has a surface tension approximately twice that of nitrogen at the test temperatures. However, if the critical surface tension is approximately equal to or greater than σ_{LV} of different liquids, then these liquids will exhibit similar and very low wetting angles. The apparently lower contact angles for oxygen as compared to nitrogen may be due to the uncoupled electrons of the oxygen interacting with the fluorine surface through coulombic forces.

There is also the possibility, as Zisman suggests, that the cryogenic fluids that were tested contained various impurities such as neon, argon, etc. The surface tension of some of these impurities could be substantially lower than that of the test liquid. It is possible then that their presence had reduced the surface tension of the liquid to approximately or even below σ_c of the test surface and consequently the small contact angles result.

With regard to the accuracy of the measurements, very small angles ($<10^{o}$) were difficult to determine exactly by the "tilting plate" technique because the effect of interference by reflections of the light beam and slight movements of the liquid surface are more pronounced at the shallow angles. Also, such small angles tend to magnify the effect of any errors in the establishment of the reference points as well as backlash in the gear system. Therefore, there is some uncertainty as to the exact magnitude of the very low angles obtained in the cryogenic tests. However, for the physical phenomena affected by wetting such

as capillary pumping, boiling, etc., the important parameter is the cosine of the contact angle. Consequently, the small errors associated with the very low angles should be insignificant in physical applications.

The cryogenic contact angle results do not absolutely rule-out the feasibility of a non-wetting cryogenic heat pipe. However, in the interest of developing a high performance static cryogenic heat transfer system within the contract period, the non-wetting concept was abandoned and the development of a cryogenic heat pipe which utilizes a "wetting arterial wick structure" was pursued.

Section 4

DEVELOPMENT OF A CRYOGENIC ARTERIAL HEAT PIPE

The "non-wetting" concept was originally selected for development because it offered potential start-up advantages in a cryogenic heat pipe. Since the efforts to establish a non-wetting cryogenic liquid/solid combination were unsuccessful, the development of a high performance cryogenic heat pipe with a "wetting" wick structure was pursued. An arterial design was selected because its ability to operate as a composite wick had been demonstrated with conventional fluids.[1] A discussion of the design, analysis, and testing of an experimental heat pipe with an arterial wick and nitrogen working fluid is given in this section.

A. Design and Analysis

An arterial wick whose cross section is shown in Figure 4-1 was inserted into a 91 cm long x 1.27 cm O.D., 6061-T6 aluminum tube. The tube has 19 approximately 0.1 mm deep screw-thread grooves per cm of length which provide circumferential distribution of the liquid. Two hundred (200) mesh stainless steel screen was used to form the 1.6 mm artery diameter. As will be discussed, the artery diameter was determined so that during start-up maximum heat transport would be provided by the open artery using nitrogen as the working fluid.

The analysis of the maximum heat transport capability of an arterial heat pipe is based on the same considerations as discussed in Section 2. In this case, however, the liquid losses dominate and the vapor transport factor (N_V) in Eq. (2-13) is replaced by the liquid transport factor N_L. Also, the effect of a gravity head is no longer negligible and must be taken into account. Thus, as derived in Ref. 2, the maximum transport capability of an artery can be determined from

FIGURE 4-1
ARTERY DESIGN

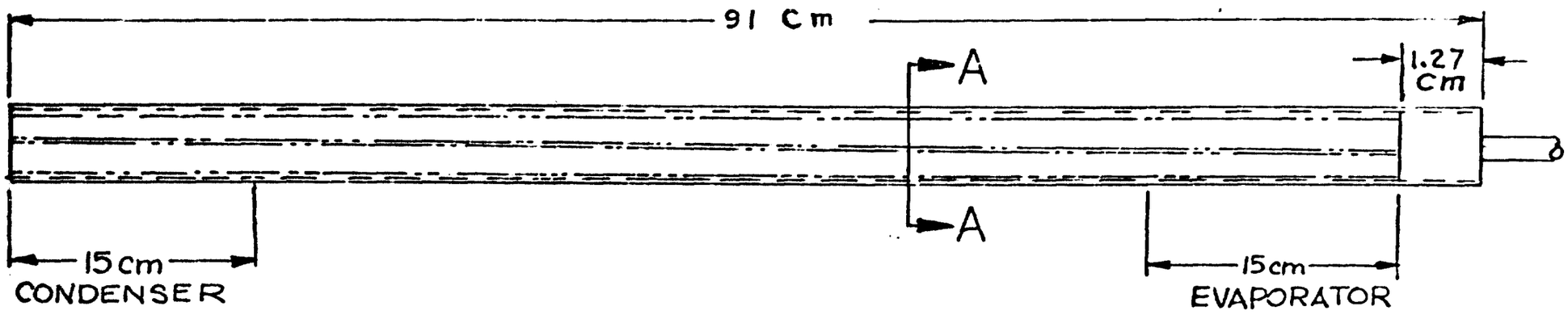

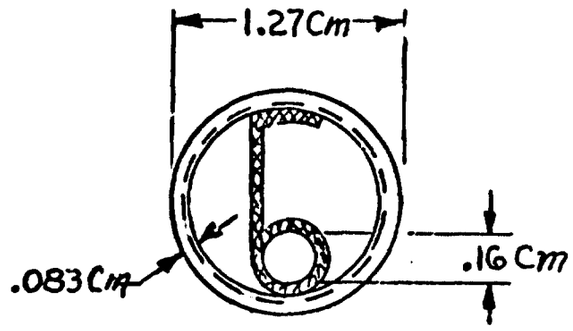

A -A

$$q L_f = \frac{(1+\eta) F_L}{16} \frac{A_L D_L^2}{r_p} N_L \qquad (4\text{-}1)$$

where $$\eta = \frac{\text{elevation head}}{\text{capillary pumping head}} = \frac{\rho_L g H}{\frac{2\sigma}{r_p}} \qquad (4\text{-}2)$$

For an artery adjacent to the wall and at the bottom of the tube, as shown in Figure 4-1, the elevation (H) is given by

$$H = n h - d_a \qquad (4\text{-}3)$$

The friction factor F_L is given by

$$F_L = \frac{\Delta p_L}{\Delta p_V + \Delta p_L} = \left[1 + \varphi \left(\frac{\sqrt{V}}{\sqrt{L}}\right) \left(\frac{D_L}{D_V}\right)^2 \left(\frac{A_L}{A_V}\right)\right]^{-1} \qquad (4\text{-}4)$$

Based on the experimental results obtained in the cryogenic contact angle tests (Section 3), it can be assumed that cos θ equals one (1) in (Eqs. (4-1) and (4-2). Also, the vapor flow area and hydraulic diameter are rather large for this design and therefore the viscous pressure drop is small compared to the liquid loss so that it can be assumed that F_L is one (1). Less than a 2% error results from this assumption.

During start-up in the cryogenic application, cooling is initiated at the condenser section where the superheated vapor loses its sensible heat and eventually begins to liquify. In an arterial heat pipe the condensed liquid advances downstream to the evaporator through the arterial channel. The rate at which the liquid advances and the ability of the artery to completely fill and perform as a composite wick is dependent upon the maximum heat transport capability of the open artery, the hydrostatic head that exists, and the parasitic heat leaks to the system. While the artery is priming, it performs like a homogeneous wick with the capillary pumping determined by the radius of the artery (i.e., $r_p = 0.5\ d_a$).

The transport capability of the open artery is therefore substantially lower than when it is fully primed and, based upon the previous assumptions, is given by

$$(q\,L_f)_{OP} = \frac{\pi d_a^{\,3}}{32}\,(1-\eta)_{OP}\,N_L \qquad (4\text{–}5)$$

with

$$\eta_{OP} = \frac{\rho_L\, g\, d_a^{\,2}}{4\sigma} \qquad (4\text{–}6)$$

Figure 4–2 shows the self-priming capacity of a horizontal heat pipe with the artery adjacent to the wall as a function of artery diameter using liquid nitrogen at 77°K. As indicated in this Figure, there is an optimum artery diameter which results in maximum transport capability during priming. This optimum is a consequence of the hydrostatic head which must be supported by the capillary pumping in a gravity field. Under zero–g conditions ($\eta = 0$) Eq. (4–5) shows that the self-priming capacity increases continuously with increasing artery diameter. The results of this analysis led to the 0.16 cm artery diameter for the experimental model.

As indicated in Figure 4–1, the wick structure extends from the end cap at the condenser section to within 1.27 cm of the evaporator end cap. It does not extend to the end cap at the evaporator to assure that the heat leak from the ambient through the fill tube would not prevent the artery from completely priming.

A hydrostatic pressure test was performed after insertion of the artery into the tube to establish the effective pumping radius of the closed artery. The artery which was filled with methanol to ensure good wetting supported a 7.5 cm column of water. The corresponding effective pumping radius as calculated from Eq. (4–7) is 5.9×10^{-3} cm.

$$r_p = \frac{2\sigma_{CH_3\,OH}}{(\rho g\, h)_{H_2O}} \qquad (4\text{–}7)$$

FIGURE 4-2

HEAT TRANSPORT CAPABILITY OF OPEN ARTERY VS. ARTERY DIAMETER

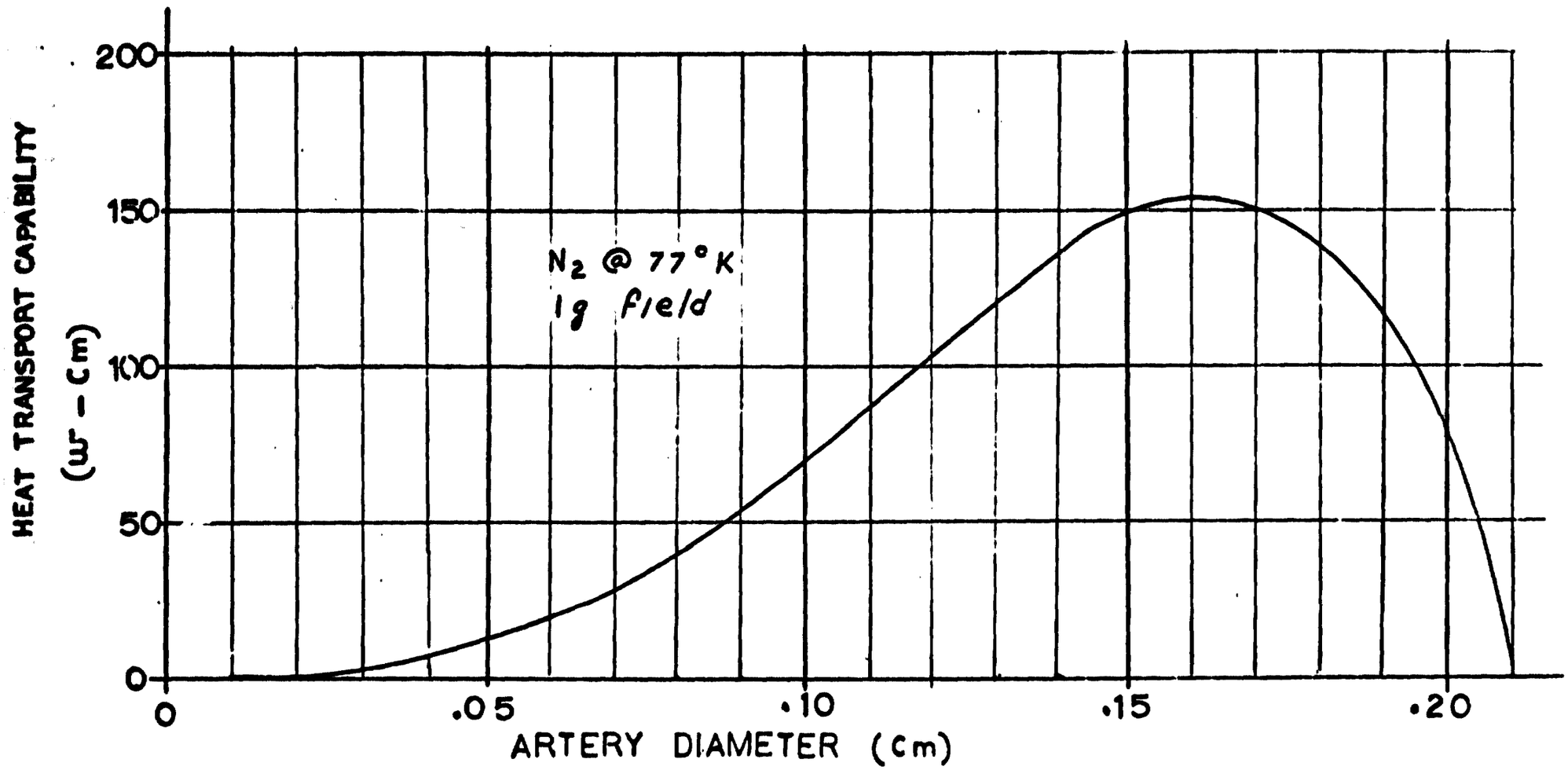

This is approximately twice the average physical pore radius of 200 mesh screen and is consistent with effective pumping radii established for various wick materials.

B. Test Setup

The heat pipe was tested in a vacuum chamber to eliminate excessive convective heat leaks. A schematic of the system is shown in Figure 4-3. All tests were conducted at a vacuum pressure of less than 20 microns with the walls of the chamber at room temperature. Prior to testing, the condenser end of the test heat pipe was inserted into a tank (approximately 2 liters) and sealed using a Swagelok fitting. The tank was used as a reservoir for the liquid nitrogen bath which served as a heat sink for the heat pipe during testing. A resistance heater, electrically insulated from the heat pipe, was wrapped around the other end of the pipe to provide a uniform heat input section. Chromel-alumel thermocouples were peened into small localized aluminum weld beads located on the outside surface of the tube. All thermocouples were located at the top of the tube during testing.

The individual heat pipe and coolant reservoir were wrapped with multilayer blankets of super-insulation, mounted on a support frame, leveled, and inserted into the chamber as shown in Figure 4-4. Once inside the chamber, the inlet and outlet ports of the reservoir were attached to vacuum feed-throughs which extend to the outside of the chamber. The inlet tube is attached via a vacuum insulated line to a liquid nitrogen storage vessel. Gaseous nitrogen is vented to the atmosphere through the outlet. A similar connection was made between a coiled stainless steel fill tube attached to the evaporator end and the external gaseous nitrogen supply. The stainless steel coil was used to minimize the heat leak to the evaporator end.

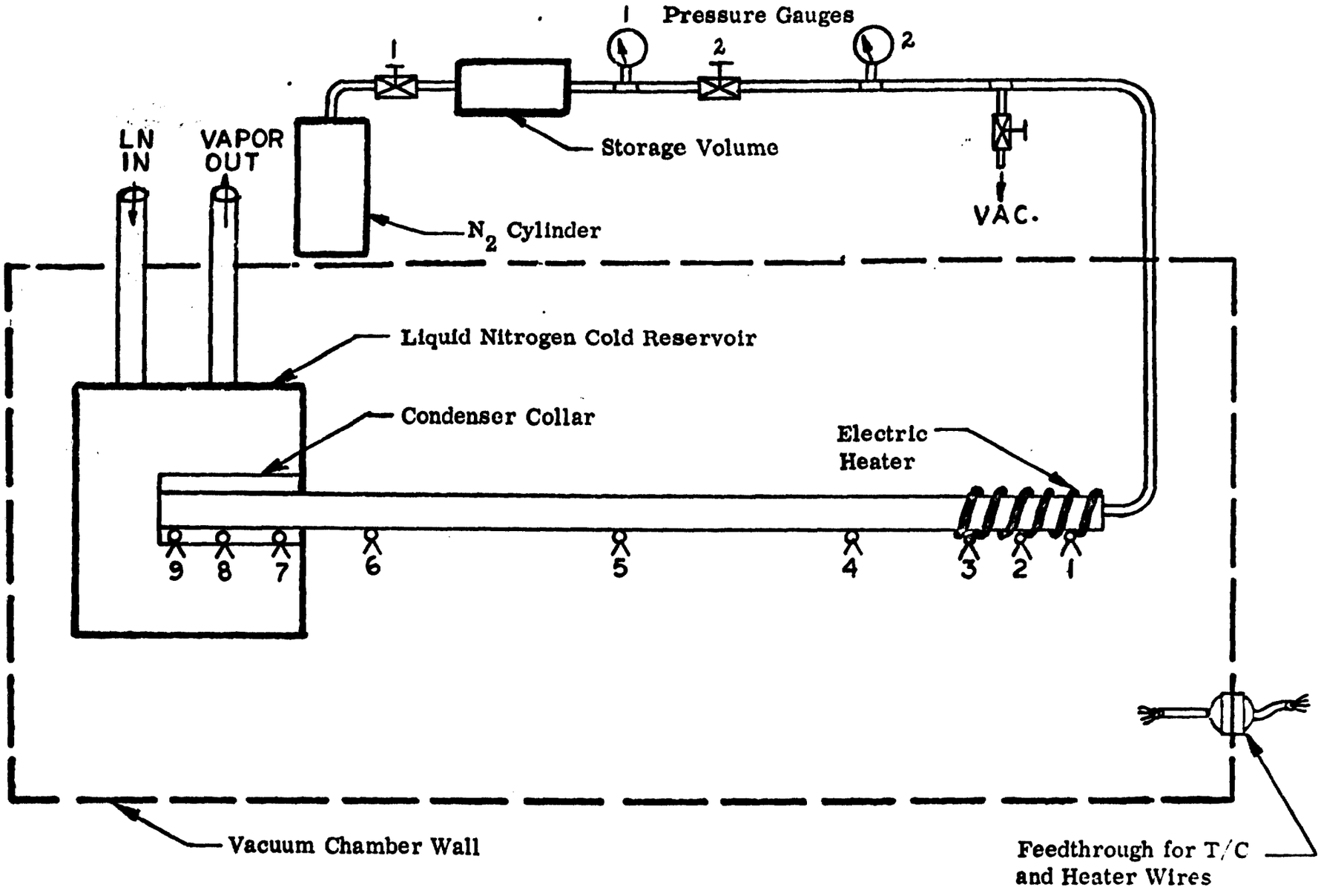

FIGURE 4-3

SCHEMATIC OF GROOVED CRYOGENIC HEAT PIPE TEST SETUP

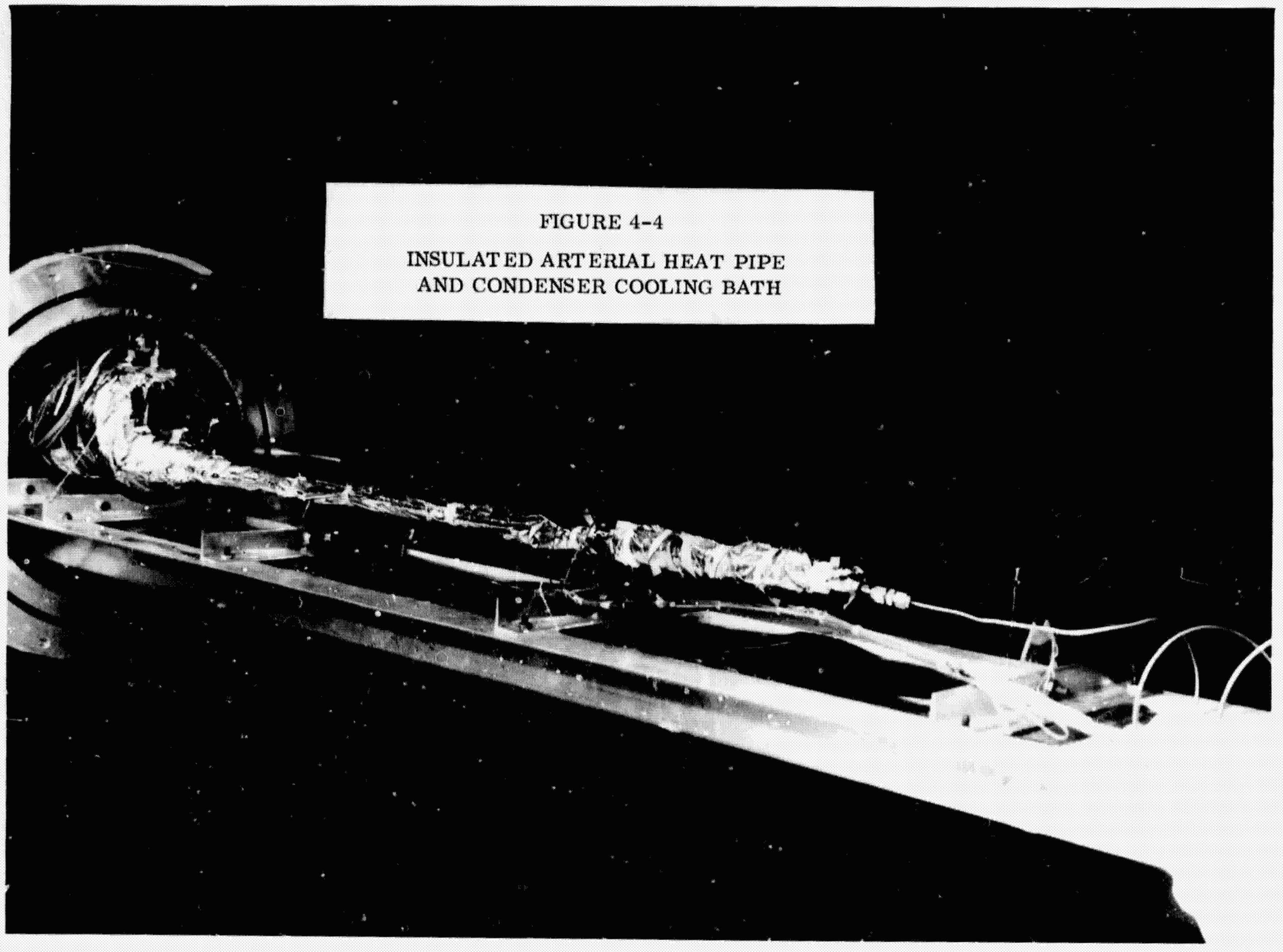

FIGURE 4-4

INSULATED ARTERIAL HEAT PIPE
AND CONDENSER COOLING BATH

Electrical feed-throughs were used to connect the heater and thermocouples to the external instrumentation. A thermocouple vacuum gauge was used to monitor the pressure within the chamber, and the pressure within the heat pipe was measured with pressure gauge #2 in Figure 4-3. The gauge adjacent to the reservoir was used to indicate the pressure of the storage volume in order to determine the amount of nitrogen gas transferred to the heat pipe.

The orientation of the heat pipe was changed by adjusting leveling pads which support the entire chamber. A surveyor's transit was used to check the level by sighting on opposite ends of the chamber.

C. Start-Up

The procedure for charging the heat pipe consists of first filling the liquid nitrogen reservoir surrounding the condenser section of the pipe, therein initiating the cooling of the pipe. A mass of nitrogen gas is then transferred from the storage reservoir to the heat pipe where it begins to fill the wick structure (either grooves or artery) and the gas-liquid interface advances toward the evaporator end. The mass of gas added to the heat pipe is determined using the Ideal Gas Law

$$m_g = \frac{\Delta p_{st} \, V_{st}}{R_g \, T_{st}} \qquad (4\text{-}8)$$

In addition to the mass of nitrogen working fluid in the heat pipe, this mass includes the nitrogen gas in lines, connectors, etc., between the evaporator end and valve #2 in Figure 4-3. However, this additional mass is very small, amounting to less than 3% of the total charge.

The start-up of the arterial heat pipe is illustrated by the data in Figure 4-5. One minute after the nitrogen gas was introduced the liquid/vapor interface had advanced

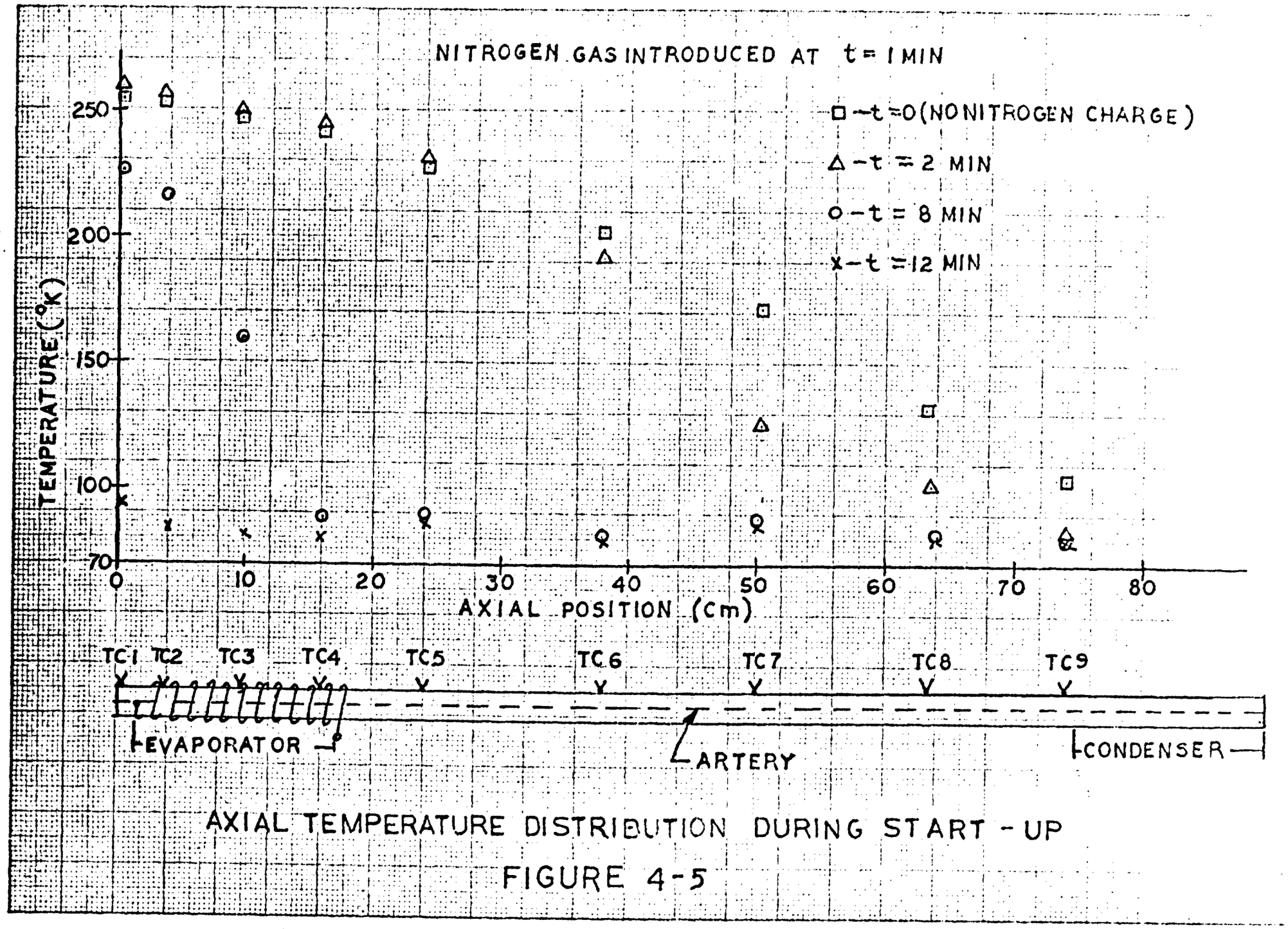

AXIAL TEMPERATURE DISTRIBUTION DURING START - UP

FIGURE 4-5

approximately 10 cm downstream from the condenser section, and the transport section had begun to cool down. The temperatures at the evaporator end experienced a slight increase initially because the nitrogen gas was somewhat warmer than the heat pipe wall. Within seven minutes the interface had advanced to the upstream end of the evaporator, and after eleven minutes the entire heat pipe was essentially isothermal at the liquid nitrogen temperature (77°K). After twenty minutes (not shown in Figure 4-5), the heat pipe was completely isothermal.

Once the heat pipe had become essentially isothermal its orientation was adjusted so that the evaporator was at some elevation above the condenser and power was applied in small increments until burnout was observed. Tests were conducted to determine the maximum heat load that could be transported at various evaporator elevations and to determine the temperature profile associated with different heat loads.

D. Test Results of Arterial Heat Pipe

The heat pipe was tested at various liquid nitrogen charges to establish the minimum charge under which the artery would prime. This minimum charge was 7.2 gms. The maximum heat transported versus elevation is shown in Figure 4-6 for the various nitrogen charges. The experimental heat transport capability is significantly lower than that predicted for an arterial pipe without screw threads. For the effective pumping radius determined from the room temperature hydrostatic test, the theoretical static elevation ($q = 0$) of the closed artery with nitrogen is 3.75 cm. This is in reasonably close agreement with extrapolation of the experimental data, and the differences could be attributed to experimental error associated with either the hydrostatic wicking test or the cryogenic tests. However, the large discrepancies between the experimental and theoretical values at the lower evaporator elevations cannot be accounted for by

FIGURE 4-6

MAXIMUM HEAT TRANSPORT VS. ELEVATION

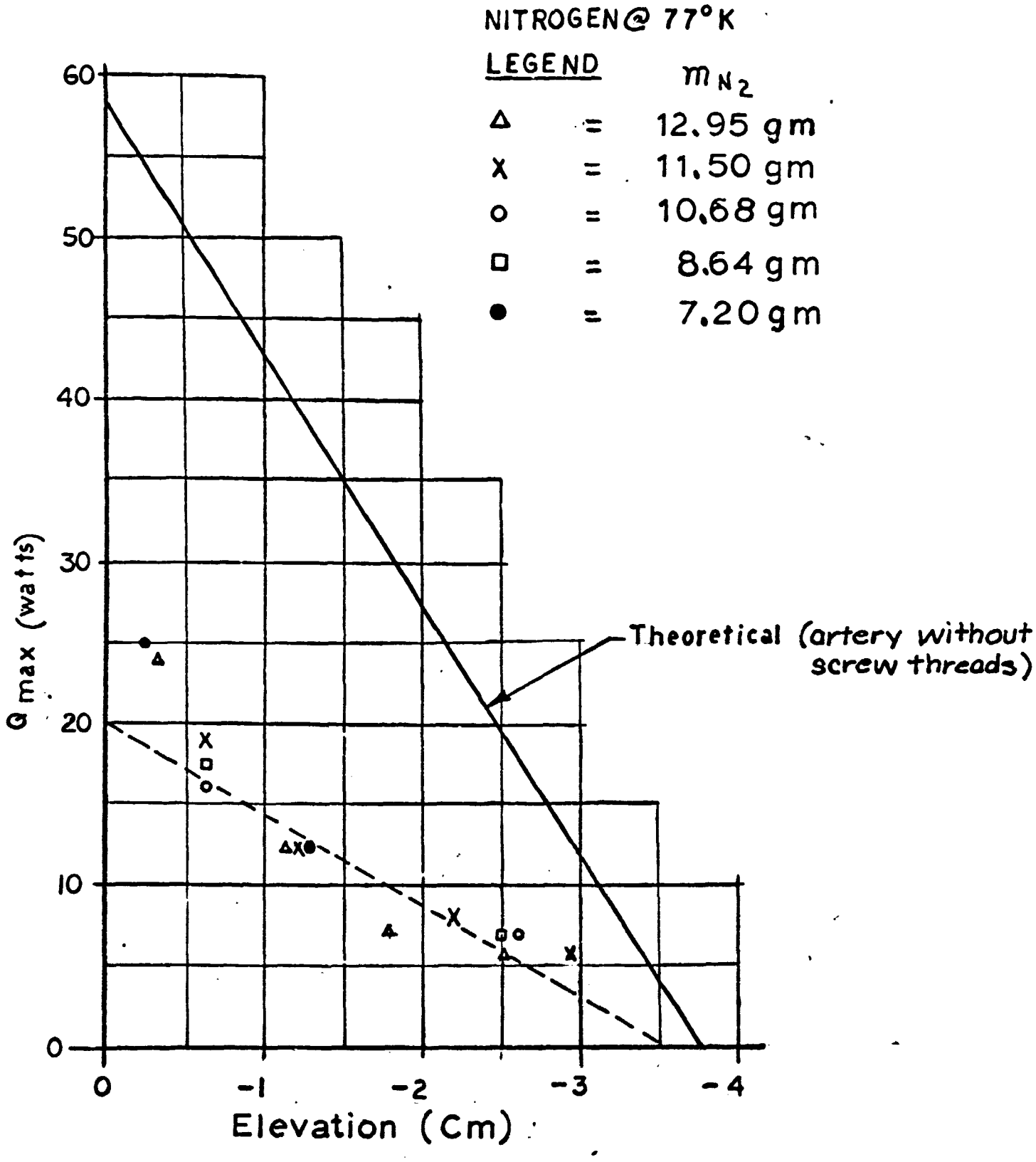

experimental error. These differences could be attributed to three factors:

(1) The screw threads are limiting the heat pipe's transport capability.

(2) Nucleate boiling at the higher heat transfer rates.

(3) A puddling effect at the lower elevations.

The possibility that the threads are limiting is indicated by the axial temperature data shown in Figure 4-7 for various power levels. As the electrical power is increased the two thermocouples located nearest to the evaporator end cap begin to rise above the other thermocouples. The first T/C is located beyond the artery and tends to indicate dry-out when power is applied. This dry-out and corresponding increase in temperature extends back to the second T/C, while the remainder of the evaporator section is isothermal with respect to the adiabatic section of the heat pipe. Only the beginning of the evaporator experiences a significant increase in temperature and therefore the artery is supplying liquid adequately to the remainder of the evaporator section. The artery must have been primed in order to sustain these heat loads with the evaporator elevated. Consequently, this drying out of the threads can only be explained by their inability to sustain the heat load and elevation head.

There is also a possibility of nucleate boiling occurring in the screw-threads at the low evaporator elevations and high heat transfer rates. The temperature drops in the evaporator initially increased linearly with heat transfer rate (Figure 4-8). As the heat transfer rate increased, however, a point was reached where the slope of the ΔT vs. heat input relationship increased. The ΔT's were not large enough to indicate that the artery had opened; and, therefore, this point could be the initiation of nucleate boiling in the screw threads. This boiling could eventually result in the opening of the of the artery and heat pipe failure.

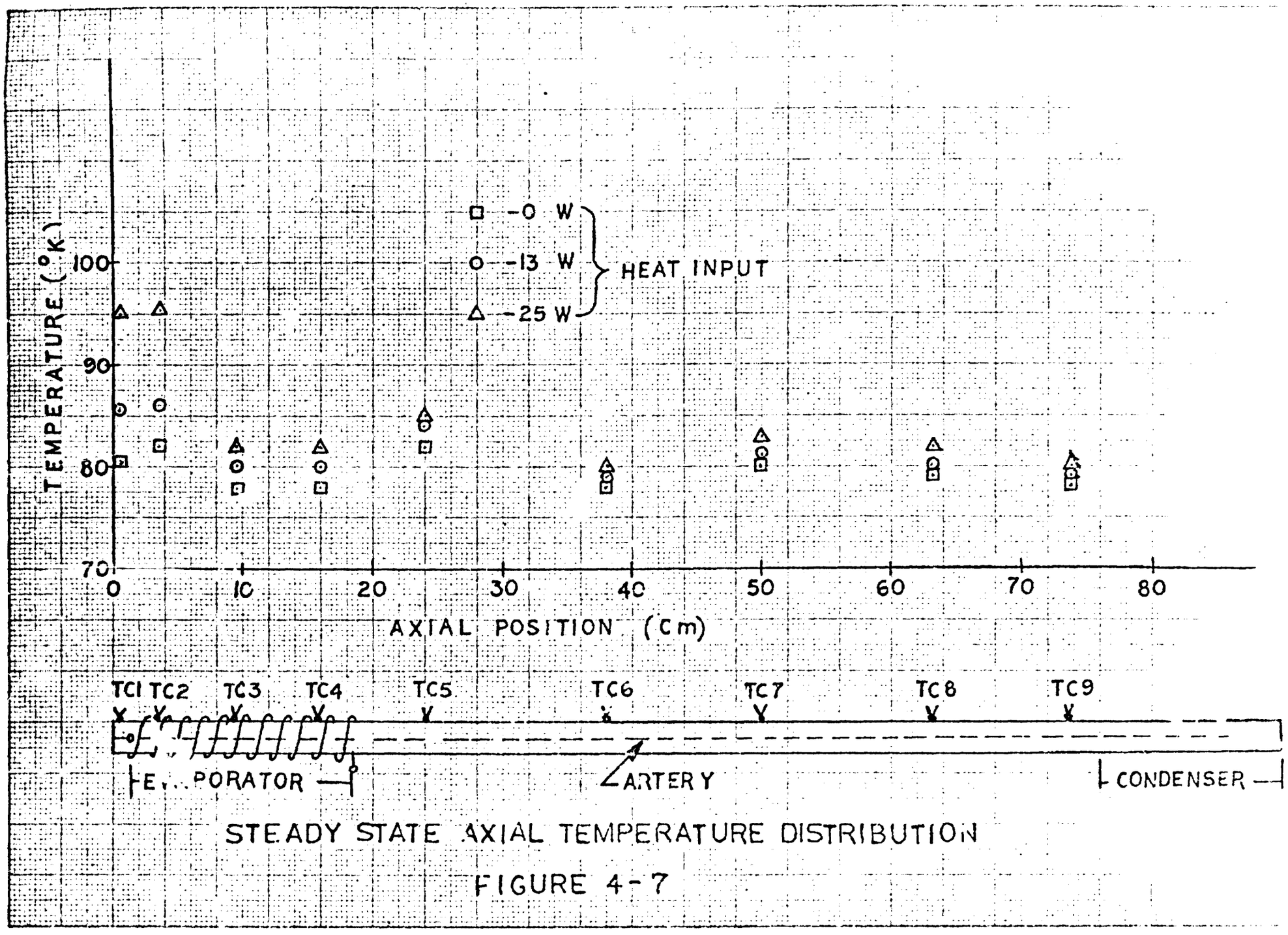

STEADY STATE AXIAL TEMPERATURE DISTRIBUTION

FIGURE 4-7

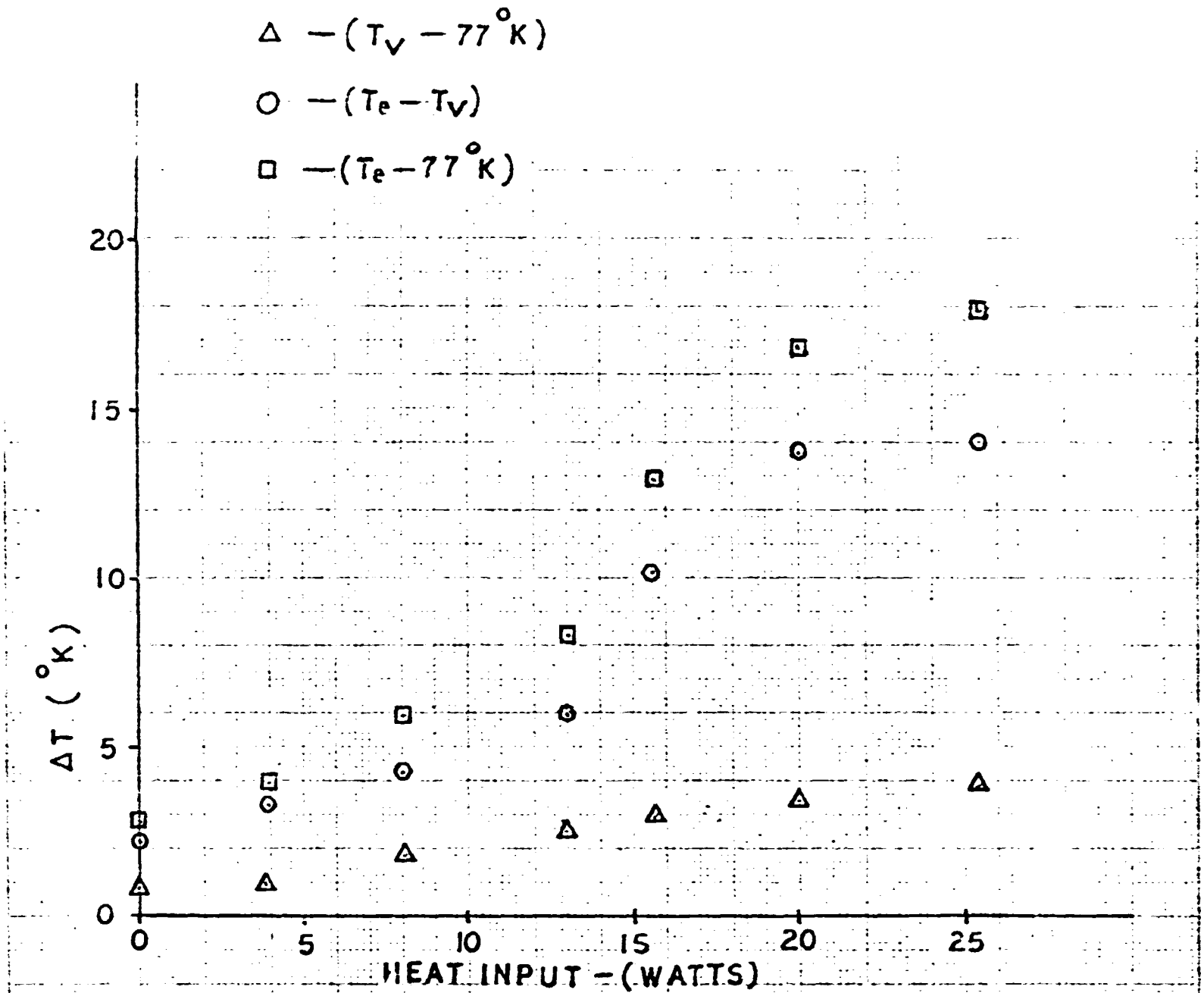

HEAT PIPE TEMPERATURE DROPS VERSUS HEAT INPUT

FIGURE 4-8

Although the screw-threads could be limiting the heat pipe's performance, the maximum heat transported should vary linearly with elevation if the capillary limit applies. However, the performance data at the lower elevations (< 0.7 cm) is somewhat better compared to a linear extrapolation of the remaining data. This improved performance is probably due to a puddling effect which is most pronounced at shallow elevations. The presence of a puddle reduces the transport length and the hydrostatic head that must be supported by the capillary pumping and hence increases the heat transport capability.

The maximum heat transport capability of this system, based on a linear extrapolation of the data, is 1500 watt-cm. After the heat pipe had burned out at the different elevations, it was releveled and allowed to isothermalize. The evaporator was then elevated to approximately 2.5 cm above the condenser, and a small amount of heat was applied to establish whether the artery had reprimed. Repeated start-up was obtained in at least 90% of the cases.

The heat pipe temperature drops vs. heat input for the tests with a 7.2 gm nitrogen charge are shown in Figure 4-8. The vapor temperature (T_V) is defined as the linear average of T/C's #6, #7, and #8. Thermocouple #5 is considered inaccurate and therefore was not included in the average. The maximum evaporator temperature drop is defined as the difference between T/C #1 and T_V; the condenser temperature drop is defined as the difference between T_V and the liquid nitrogen bath (77°K); and the maximum temperature drop across the heat pipe is defined as the sum of the evaporator and condenser temperature drops.

The maximum evaporator temperature drop varies linearly with heat input up to approximately 14 watts with a corresponding conductance of .058 watts/cm^2-°C (100 BTU

per hr-ft^2-^{o}F). Above 14 watts the temperature difference increases abruptly, indicating a partial dry-out of the screw-threads.

The condenser temperature drop varies linearly with input power from 1^{o}C at 4 watts to 4^{o}C at 25 watts. Since this difference includes the temperature drop between the outer wall of the condenser section and the liquid nitrogen bath, the minimum condenser conductance for this design is 0.116 watts/cm^2-^{o}C (200 BTU/hr-ft^2-^{o}F). The total temperature drop increases from 4^{o}C at 4 watts to 18^{o}C at 25 watts.

Section 5

CONCLUSIONS AND RECOMMENDATIONS

The use of a non-wetting wick structure has potential start-up advantages in a cryogenic heat pipe since full pumping power is available upon the onset of condensation of the cryogenic working fluid. However, contact angle measurements of liquid nitrogen, oxygen, and Freon 13 on various low energy surfaces which have the best potential for being non-wetting were all less than 30^{o}. Since contact angles greater than 90^{o} are required for non-wetting, the development of a heat pipe which employs a wetting arterial wick was pursued because of its potential high performance capability. Performance tests were conducted with an experimental heat pipe whose arterial wick had been designed such that during start-up maximum heat transport would be provided by the open artery using nitrogen as the working fluid. Once primed, the cryogenic arterial heat pipe exhibited a heat transport capability well in excess of the projected requirements for spacecraft applications using cryogenic heat pipes. This high performance was combined with a good overall thermal conductance and a relative insensitivity to gravity.

The following tasks are recommended to further the development of cryogenic arterial heat pipe technology:

- Perform additional tests with the experimental model to establish the reliability of start-up
- Perform further analysis to account for the effect of the screw threads on the heat pipe's heat transport capability
- Formulate an analytic model which predicts the transient performance of a cryogenic heat pipe system
- Design, fabricate, and test a second generation arterial heat pipe which has been optimized for maximum heat transport based on the results of the preceding tests and analyses.

Section 6

NEW TECHNOLOGY

The experimental heat pipe developed under this program was the first heat pipe which employs an arterial wick to have been proven operational at cryogenic temperatures. The arterial wick operates on the "composite wick principle" and is therefore capable of significantly better performance than that afforded by conventional wick structures. This improved performance includes high heat transport capability combined with high overall thermal conductance and relative insensitivity to gravity.

REFERENCES

1. Bienert, W. B., and Kroliczek, E., "Experimental High Performance Heat Pipes for the OAO-C Spacecraft," ASME Paper No. 71-AV-28. July 1971.

2. Frank, S., et al, "Heat Pipe Design Manual," MND-3288, Martin Marietta Corp., 1967.

3. Scheidegger, A. E., "The Physics of Flow Through Porous Media," MacMillan Co., New York, 1960.

4. RCA, Advanced Technology Laboratories, "ICICLE Feasibility Study," Final Report, Radio Corporation of America, Camden, New Jersey, 1970.

5. Levy, E. K., "Investigation of Heat Pipes Operating at Low Vapor Pressures," Proc. Annual Aviation and Space Conference, California, ASME (1968), p. 671.

6. Young, T., Phil. Trans. Roy Soc. 95, 1805. p. 84

7. Dupre, A., "Theorie Mechanique de la Chaleur," Gauthier-Villars, Paris, 1869. p. 369.

8. Bangham, D. H., Trans. Faraday Soc. 33, 1937. p. 805

9. Wenzel, R. N., Ind. Eng. Chem. 28, 1936. p. 988

10. Levine, O., Zisman, W. A., Journ. Phys. Chem. 61, 1957. p. 1068

11. Zisman, W. A., "Contact Angle, Wettability, and Adhesion," Fowkes, F. M., ed. Advanced Chemistry Series No. 43, American Chemical Society, Wash., D. C., 1964. pp 1-51

12. Shafrin, E. G. and Zisman, W. A., op. cit. p. 145-157

13. Hare, E. F., Shafrin, E. G., and Zisman, W. A., Jour. Phys. Chem. 58, p. 236.

14. Griffith, A. A., Phil. Trans. Roy. Soc. London, A221, 1920. p. 163

15. Burnett, M. K., Zisman, W. A., Jour. Phys. Chem. 65, 1961. p. 2266

16. Fox, H. W., Zisman, W. A., Jour. Colloid Sci. 5, 1950. p. 512

17. Shafrin, E. G., Zisman, W. A., Jour. Phys. Chem. 61, 1957. p. 1046

18. Ibid 7, 1952. p. 428

19. Shafrin, E. G., Zisman, W. A., Jour. Colloid Sci. 4, 1949. p. 571

20. Bennett, M. K., Zisman, W. A., Jour. Phys. Chem. 66, 1962. p. 1207

21. Ellison, A. H., Zisman, W. A., Jour. Phys. Chem. 58, 1954. p. 260

22. Shafrin, E. G., Zisman, W. A., Jour. Phys. Chem. 64, 1960. p. 519

23. Spreece, A. L., et al, Rev. Sci. Instr. 28, 1957. p. 636